TITLE: COST-EFFECTIVE METHOD FOR PRODUCING SELF SUPPORTED PALLADIUM ALLOY MEMBRANES FOR USE IN EFFICIENT PRODUCTION OF COAL DERIVED HYDROGEN

FINAL TECHNICAL REPORT

REPORTING PERIOD START DATE:	9/09/03 (PROGRAM START)
REPORTING PERIOD END DATE:	3/31/08
PRINCIPLE AUTHOR(S):	K. COULTER
DATE REPORT WAS ISSUED:	JUNE 2008
DOE AWARD NUMBER:	DE-FC26-03NT41849
SUBMITTING ORGANIZATION:	SOUTHWEST RESEARCH INSTITUTE® 6220 CULEBRA ROAD (78238-5166) P.O. BOX 28510 (78228-0510) SAN ANTONIO, TEXAS
OTHER TEAM MEMBERS:	COLORADO SCHOOL OF MINES IDATECH, LLC
SUBMIT TO:	NETL AAD DOCUMENT CONTROL BLDG. 921 U.S. DEPARTMENT OF ENERGY NATIONAL ENERGY TECHNOLOGY LABORATORY P.O. BOX 10940 PITTSBURGH, PA 15236-0940

SOUTHWEST RESEARCH INSTITUTE®
SAN ANTONIO, TEXAS HOUSTON, TEXAS WASHINGTON, DC

TITLE: COST-EFFECTIVE METHOD FOR PRODUCING SELF SUPPORTED PALLADIUM ALLOY MEMBRANES FOR USE IN EFFICIENT PRODUCTION OF COAL DERIVED HYDROGEN

FINAL TECHNICAL REPORT

REPORTING PERIOD START DATE:	9/09/03 (PROGRAM START)
REPORTING PERIOD END DATE:	3/31/08
PRINCIPLE AUTHOR(S):	K. COULTER
DATE REPORT WAS ISSUED:	JUNE 2008
DOE AWARD NUMBER:	DE-FC26-03NT41849
SUBMITTING ORGANIZATION:	SOUTHWEST RESEARCH INSTITUTE 6220 CULEBRA ROAD (78238-5166) P.O. BOX 28510 (78228-0510) SAN ANTONIO, TEXAS
OTHER TEAM MEMBERS:	COLORADO SCHOOL OF MINES IDATECH, LLC
SUBMIT TO:	NETL AAD DOCUMENT CONTROL BLDG. 921 U.S. DEPARTMENT OF ENERGY NATIONAL ENERGY TECHNOLOGY LABORATORY P.O. BOX 10940 PITTSBURGH, PA 15236-0940

APPROVED:

BEN H. THACKER, DIRECTOR
MATERIALS ENGINEERING DEPARTMENT

DISCLAIMER

"This report was prepared as an account of work sponsored by an agency of the United States Government. Neither the United States Government nor any agency thereof, nor any of their employees, makes any warranty, express or implied, or assumes any legal liability or responsibility for the accuracy, completeness, or usefulness or any information, apparatus, product, or process disclose, or represents that its use would not infringe privately owned rights. Reference herein to any specific commercial product, process, or service by trade name, trademark, manufacturer, or otherwise does not necessarily constitute or imply its endorsement, recommendation, or favoring by the United States Government or any agency thereof. The views and opinions of authors expressed herein do not necessarily state or reflect those of the United States Government or any agency thereof."

ABSTRACT

Southwest Research Institute® (SwRI®) has utilized its expertise in large-area vacuum deposition methods to conduct research into the fabrication of dense, freestanding Pd-alloy membranes that are 3-5 microns thick and over 100 in^2 in area. The membranes were deposited onto flexible and rigid supports that were subsequently removed and separated using novel techniques developed over the course of the project. Using these methods, the production of novel alloy compositions centered around the Pd-Cu system were developed with the objective of producing a thermally stable, nano-crystalline grain structure with the highest flux recorded as 242 SCFH/ft^2 for a 2 μm thick $Pd_{53}Cu_{47}$ at 400°C and 20 psig feed pressure which when extrapolated is over twice the 2010 Department of Energy pure H_2 flux target. Several membranes were made with the same permeability, but with different thicknesses and these membranes were highly selective. Researchers at the Colorado School of Mines supported the effort with extensive testing of experimental membranes as well as design and modeling of novel alloy composite structures. IdaTech provided commercial bench testing and analysis of SwRI-manufactured membranes. The completed deliverables for the project include test data on the performance of experimental membranes fabricated by vacuum deposition and several Pd-alloy membranes that were supplied to IdaTech for testing.

Table of Contents

List of Tables

List of Figures

List of Figures (Continued)

List of Figures (Continued)

INTRODUCTION

Coal gasification and fuel cells are two of our nation's most promising technologies for the efficient production of clean electricity. At the heart of these technologies is hydrogen. Unfortunately, the ability to produce pure hydrogen has been a particular challenge that has impeded progress in both areas and will only become a more significant issue in the years ahead. Hydrogen is costly to produce or to separate from gas mixtures such as reactor effluent or waste streams due to the high capital and energy expenditures associated with compression, heat exchange, cryogenic distillation, and Pressure Swing Adsorption (PSA).

An affordable, tough, and selective hydrogen separating membrane could significantly reduce these costs, and ultimately replace traditional unit operations or be integrated into an existing process to recover hydrogen. Polymer membranes represent one type of commercially available membrane that currently compete with the other technologies to reduce the hydrogen/carbon monoxide ratio in synthesis gas (syngas), or to recover hydrogen from purge of off-gas streams in ammonia or petrochemical plants. Polymer membranes are economical in some applications, but the higher temperatures of most chemical reactions and many waste gas and reforming (i.e., coal gasification/natural gas) streams precludes their use, at least without process modifications such as cooling prior to introduction into the module. In general, polymer membrane systems require lower capital investment although their primary liability is the recompression of the permeated hydrogen is usually required.

Considerable research in the area of inorganic membranes for hydrogen gas separation for purification at high temperatures has taken place in recent years, much of which has been supported by DOE. Ceramic high-temperature membranes have been developed and commercialized for gas separation. Typically the ceramics must exhibit an extremely fine, highly controlled pore size that can be difficult to fabricate over large areas. In addition, the mechanical integrity of a thin ceramic membrane is suspect in the harsh environment associated with coal gasification and some of the ceramics being considered are exotic and expensive to make. Hence, the ability to manufacture ceramic membranes at a low cost and in a continuous process has yet to be fully established.

Metal membranes appear to have advantages over ceramic and polymer membranes in terms of manufacturability, lifetime (durability), higher operating temperatures and selectivity. Of the metal membranes, self-supporting, dense palladium alloy membranes have been shown to exhibit extremely high hydrogen selectivity and are able to produce high purity hydrogen feed streams needed for fuel cell applications, although they have yet to be extensively realized on a commercial scale. Other unique benefits that palladium foils offer are that they can be configured to perform multiple functions and thereby reduce overall reactor costs. For example, as a palladium membrane reactor, chemical (especially catalyzed) reactions and product purification can be used to add or remove hydrogen to drive equilibrium restricted reactions to the desired product side. As a result of this added feature, reactor volume and temperature may be lowered, undesirable byproducts formation through side reactions reduced, and lower un-reacted feed for recycling; all of these added features ultimately leading to savings on downstream separation requirements, equipment size, and energy usage [1,2].

A robust, hydrogen selective palladium membrane, therefore, has the potential to change the chemical industry by replacing traditional reaction and separation procedures, resulting in sizable savings in energy consumption and capital investment in equipment. This increased functionality and energy saving benefit in combination with high hydrogen selectivity and flux, at a cost comparable with polymer membrane technology, make palladium membranes an attractive hydrogen separation technology.

Palladium as a Membrane Material

Although palladium membranes have potential for efficient and economical separation of hydrogen from mixed gas streams produced by coal gasification, a major shortcoming of palladium as a membrane material is the high and fluctuating cost and the difficulty of fabricating robust, defect-free membranes thinner than 15 microns. Reducing the thickness of palladium is not only an issue of cost, but performance since permeability is inversely proportional to palladium film thickness; i.e., to compete with state of art methane steam reforming, it is estimated that the palladium thickness must be around 2 microns.

Self-supporting dense palladium alloy membranes can provide adaptability to a variety of system sealing configurations with high selectivity although fabrication of a thin (<25 μm) pinhole-free, free-standing membranes with stable, predictable performance over a long period of time at high temperatures has been a challenge. Since the long term stability of pure palladium at high temperatures (>450ºC) has been a problem, due to poisoning (carbon deactivation/sulfur) and phase transformations (leading to warping and embrittlement), palladium is typically alloyed with other elements, such as silver (Ag), ruthenium (Ru), and copper (Cu) to stabilize the structure and minimize poisoning effects. Alloying improves mechanical stability and has also been shown to increase hydrogen permeability [3].

The most common approach to fabricating dense metal membranes has been to apply conventional rolling processes to "squeeze" a metal foil as thinly as possible. The potential for pinhole defects limits this method for Pd-alloy membranes to a current state of the art of 15 μm. Difficulty in controlling deformation across the length of the press rolls used in forming the membranes limits the practical width of the membranes. Other methods, such as traditional "thick-film" coating techniques, have been used to fabricate self-supporting membranes. Coating methods, such as electroplating and electroless deposition, have been demonstrated but have significant concerns with contamination from organic carbon and the ability to keep a controlled and consistent bath chemistry over multiple cycles and large areas [4].

Vacuum-Deposited, Thin-film Palladium Membranes

Vacuum deposition methods are used in a wide variety of industries including semiconductors, machine tools, and packaging. At a manufacturing level, vacuum-based processes can be cost-effective. A limited amount of work has been reported on the fabrication of palladium membranes using vacuum deposition methods and of these [5], the emphasis has been on using supported metal/ceramic substrates to create the composite membrane structures. Palladium films deposited on iron by RF sputtering (0.68 to 1.36 μ thick) and e-beam evaporation (0.022 – 0.135 μ thick)

were found to have hydrogen diffusivities ~2 orders of magnitude lower than bulk, free-standing, palladium. The reduced performance was due to the large number of lattice defects and grain boundaries (area) and in the case of e-beam evaporated palladium films, the decrease in hydrogen diffusivity was attributed to an increase in hydrogen solubility; i.e., possibly due to excess "traps" or defects such as dislocations and vacancies.

A vacuum-based process must be capable of: (1) enhancing catalyst activity/site number at surface while reducing impurities, (2) optimizing diffusion pathways/hydrogen permeation in the bulk, and (3) reproducibly producing cost-effective, thin, dense, self-supporting films for manufacturing, in order to successfully create a more efficient/cost-effective hydrogen separation membrane. Of the vacuum deposition techniques that are scaleable, Physical Vapor Deposition (PVD) methods provide the greatest level of control of membrane properties through control of composition and incident atom/ion energetics. This is the kind of control that cannot only enhance membrane performance, but "bridge" the lab-scale level of development into a reproducible manufacturing process. Magnetron Sputtering is a method with the ability to deposit alloy films of virtually any composition over large areas by simply constructing a target of the appropriate size and composition. Because of the energetics of the technique, dense, pinhole-free films can be formed at low temperatures and reasonably high deposition rates. Using this method, Pd-alloy films can be deposited at thicknesses ranging from as much as 10-12 μm to possibly as thin as 1-2 μm and thereby reduce, by as much as an order of magnitude, the precious metal content of a hydrogen purification system.

Clearly, freestanding membranes cannot be directly fabricated by PVD. A rather novel approach is to select and use a suitable temporary substrate that can be easily and cleanly removed after processing, leaving a freestanding membrane. Important requirements for the substrate material are that it be very smooth and free of contaminants, pinholes, and surface defects. The materials also must have decent thermal stability and be inexpensive (relative to the membrane), reusable, and/or recyclable.

Keeping in mind all the aforementioned issues, the objectives of the program were identified as:

1) Develop process methodology for the cost-effective manufacturing of thin, dense, self-supporting palladium alloy membranes for hydrogen separation from the mixed gas streams of coal gasification; reduce thickness by >50% over current state of the art.
2) Demonstrate viability of using ion-assisted, vacuum processing, to "engineer" a membrane microstructure/surface that optimizes hydrogen permeability/separation and lifetime.
3) Demonstrate efficacy of continuous roll-to-roll manufacturing of membrane material with performance/yields within pre-defined tolerance limits; establish "scale-independent" correlations between membrane properties and processing parameters.
4) Demonstrate separation efficiency of thin palladium membrane in commercial-type fuel processor (i.e., IdaTech) using mixed gas stream derived from coal gasification.
5) Develop cost model for hydrogen production from coal gasification using Pd membrane.

Based on the identified objectives, the anticipated deliverables for this project included performance data on SwRI-developed experimental membranes and a robust cost effective manufacturing concept for fabrication of these membranes in practical quantities. In addition, several large area (up to 75 in^2) thin (less the 10 μm) Pd-alloy membranes were provided to IdaTech for testing and evaluation, either as individual test articles or as part of a prototype hydrogen purification system.

EXECUTIVE SUMMARY

Coal gasification and fuel cells are two of our nation's most promising technologies for the efficient production of clean electricity. At the heart of these technologies is hydrogen. Unfortunately, the ability to produce pure hydrogen has been a particular challenge that has impeded progress in both areas. A robust, hydrogen selective palladium membrane, therefore, has the potential to change the chemical industry by replacing traditional reaction and separation procedures, resulting in sizable savings in energy consumption and capital investment in equipment. This project has demonstrated the use of vacuum deposition methods as a cost effective approach to manufacture palladium alloy membranes for efficient and economical separation of hydrogen from mixed gas streams.

The novel feature of the SwRI approach was to prepare freestanding, thin membranes by vacuum deposition on to a suitable temporary substrate that was easily and cleanly removed. Important requirements for the substrate material were that it be smooth and free of contaminants, pinholes, and surface defects. The materials also had to have decent thermal stability and be inexpensive (relative to the membrane), reusable, and/or recyclable. Based on these requirements, two initial approaches were investigated; 1) deposition of the membrane onto a polymeric substrate, which was subsequently chemically dissolved and 2) deposition onto a rigid substrate with and without pretreatment of a thin release coating.

The initial alloy coatings deposited on to polymers showed a tendency to exhibit pinhole defects most of which were attributed to the presence of dust particles. As an alternative method to address the issue of defects in the Pd-Cu alloy membrane films, films were deposited onto smooth, silicon wafers. Particulate and other contaminants were more readily controlled (i.e., minimized) on a silicon surface in comparison to plastic, and was considerably smoother than plastic. In general, the key factors that affected formation of a thin, dense, defect-free, Pd-Cu alloy films were surface energy, roughness, and oxygen/moisture content of the backing material. Correspondingly, using vacuum processing conditions that were optimized to minimize intrinsic film stress, pinhole-free Pd-Cu alloy films over large areas at thicknesses below 5 μm were produced.

As-deposited membranes were in the alpha phase and transformed to a beta or mixed alpha and beta phase upon heating to 400°C. Because these membranes were very thin it was a concern that assembly of the membranes into a module while still in the fcc phase and the change in lattice parameter associated with the phase transformation would result in a contraction that would place stress on the membrane and cause it to rupture. A series of annealing experiments were completed to convert the membrane to the desired phase prior to assembly in a module. X-ray Diffraction (XRD) showed that the as-deposited membranes were in the pure alpha phase while the annealed samples were purely beta. SEM images indicated that the membrane was unchanged during the annealing process.

To test the hydrogen permeation, a membrane foil was sandwiched between two circular supports, such as alumina paper, and then sealed with either a Kalrez O-ring (max. use to 315°C) or Grafoil packing material (allowing a 650°C upper use temperature in oxygen-free environments) in a 25 mm Millipore membrane cell. The membrane was then checked with helium to confirm a tight seal and that the membrane was defect (pinhole) free. Subsequently, the membrane was heated to operating temperature to begin permeation testing.

An example of a successful membrane was a 12.7 μm thick foil with a composition slightly off the ideal $Pd_{60}Cu_{40}$ (i.e., slightly higher palladium weight fraction). The membrane was heated to 250°C, and the hydrogen permeability at this temperature was determined to be $3.8 \cdot 10^{-5}$ $cm^3(STP) \cdot cm/cm^2 \cdot s \cdot cm\ Hg^{0.5}$. This is good agreement given that the palladium composition of the foil sample is higher than 60 mass % and that the H_2 permeability declines sharply for higher Pd contents. A range of palladium compositions and thicknesses were tested at Colorado School of Mines (CSM) under typically 400°C and 20 psi trans-membrane pressure. The following table shows the how the extrapolated hydrogen flux of a representative SwRI membrane compares to the targets established by the Office of Fossil Energy Hydrogen from Coal RD&D plan.

Performance Criteria	**Membrane *SwRI-pg168***	**2007 Target**	**2010 Target**	**2015 Target**
Flux scfh/ft^2 @ 100 psi ΔP H_2 partial pressure & 50 psia permeate side pressure	564	100	200	300

While CSM was able to measure a significant number of thin foils using their experimental gasket set-up, IdaTech was not able to successfully assemble a module that would meet IdaTech's allowable leak rate requirements and did not pursue assembly of a fuel processor with the SwRI membrane. Fabrication of a module utilizing the SwRI foils will require significant development of a new gasket compression process or alternative module design.

Of the elements that comprise a hydrogen purification module, the membrane is presumed to be by far the most significant cost contributor. The total cost for manufacturing is based on the raw materials cost, annual equipment depreciation, labor costs, utilities and maintenance, and throughput. Using industry accepted rates, a total cost of $45.40 per square foot for a vacuum deposited membrane was calculated. Even if the rates for throughput, equipment, or labor costs are significantly underestimated, this estimate is more than an order of magnitude lower than the DOE 2010 target.

In this program, self-supporting Pd-Cu alloy membranes have been produced with thicknesses down to 3 μm. Hydrogen permeability rates in excess of the 2010 DOE Targets have been measured and self-supporting membranes that exhibit long life at temperatures above 300°C were produced. It has been shown to be feasible to produce membranes below 5 μm in thickness that are competitive with other methods for hydrogen separation in energy applications. The program is well positioned for pilot scaling and membrane incorporation in commercial separation units.

EXPERIMENTAL

The majority of the effort was conducted at SwRI in San Antonio, Texas. SwRI is one of the original and largest independent, nonprofit, applied research and development organizations in the United States. It was founded in 1947 as a nonprofit corporation to provide contract research and development services to industrial and government clients. The Institute consists of 11 technical divisions that offer multidisciplinary, problem-solving services in a variety of areas in the physical sciences and engineering. The Institute's total revenue for fiscal year 2007 was $500 million. The staff of 3,100 specialize in the creation and transfer of technology in engineering and the physical sciences. Nearly 2 million square feet of office and laboratory space are maintained on a 1200 acre site.

The Surface Engineering Laboratories comprise over 2,000 sq. ft. of facilities dedicated to plasma based modification and coating of advanced materials. With its full compliment of deposition and coating technologies, including ten vacuum coating chambers with some that are 3 cubic meters in size, the Surface Engineering Group is able to satisfy customer coating needs through controlled engineering of surface properties. Using PVD processes, such as magnetron sputtering and e-beam evaporation, film properties, such as morphology/texture, intrinsic stress, composition, and density can be reliably controlled within the plane of the surface (spatially) as well as through-the-thickness of the film ("z-grading"). Films can be deposited onto large complex shapes as well as onto continuous web configurations. The primary chamber utilized for this project is shown in Figure 1a with the interior shown in 1b.

a) b)

Figure 1. a) Mill Lane Vacuum Coating Platform, b) plasma cleaning & magnetron set-up

An overview of the team capability is presented in Table 1 below. In addition to the equipment and facilities listed, IdaTech also offers experience with commercialization of fuel processors.

Table 1. List of Equipment/Facilities for each Team Member

Organization	Equipment/Facilities	Unique Capabilities
SWRI (Additional Support)	Vacuum/Inert Atmosphere Furnace Differential Scanning Calorimetry AFM/FTIR Spectroscopy SEM, XRD, Scanning AES	Material Characterization
CSM Chemical Engineering & Process Research Center (CEPR)	Automated, High Pressure, High Temperature Gas Flow Systems (3) HP 5890 Series II Gas Chromatograph TGA/DTA, FTIR, GC/5073 MS Detector Rotating Ellipsometer Analyzer Coulter Omnisorp 100 Pore Site Analyzer	**Diffusion Rate Experiments** • Porous Materials • Various Geometries, – Flat Sheet – Hollow Fiber – Tubular • Toxic Gases
IdaTech	Facility For Developing and Testing Integrated Steam Reformers/Hydrogen Purifiers For Low Temp. Fuel Cells (i.e., PEM)	**Manufacturer Fuel Processors:** • Over 150 Units • >99.95% Hydrogen Purity With <1 Ppm CO And <5 Ppm CO_2 (Rejection Of All Other Impurities) • Demonstrated Fuel Types: Natural Gas, Propane, Diesel, Synthetic Diesel, Gasoline, Fischer-Tropsch Liquids, Bio-Diesel, K1 KeroseneColeman White Gas, Ethanol/Methanol

The composite membranes fabricated at SwRI were extensively characterized using nitrogen leak testing, Scanning electron microscopy (SEM)/ energy dispersive X-ray (EDX), and X-ray diffraction (XRD). Membranes were leak-tested by pressurizing the feed side of a dead-end permeation cell with N_2 and measuring the time for the pressure to decay from 130 to 120 psig. Membranes showing low nitrogen leakage rate, less than 5×10^{-5} mols/m^2/s, were tested at high temperatures. The membrane alloy composition was verified by both SwRI and CSM by XRD and SEM/EDX. Cross sections of the film were analyzed by EDX to obtain concentration profiles and observe if intermixing of the components was achieved. XRD was also employed to determine the exact alloy composition, the lattice parameter, and grain size using established methods. SEM was used to observe film morphology including adherence to the support, grain size, and formation of porosity.

Pure gas hydrogen and nitrogen permeation rates were determined at CSM for a range of pressure differentials (5 to 50 psig feed pressure) and temperatures ranging from 200 to 600°C to evaluate performance and to screen possible membrane reactor applications. To enable permeation testing of the membranes at high temperatures (up to 450°C), a high temperature, pure gas transport apparatus was assembled and feasibility of the apparatus was demonstrated by pre-annealing and testing a 25 μm-thick, commercially available, $Pd_{60}Cu_{40}$ alloy foil from Wilkinson Company of

Post Falls, Idaho. Commercially available Grafoil valve packing material (Figure 2) was used to seal the 25 mm Millipore membrane cell, allowing a 650°C upper use temperature in oxygen-free environments. A membrane foil was sandwiched between two circular supports, such as alumina paper, and then sealed with either a Kalrez O-ring (max. use to 315°C) or Grafoil packing material in the 25 mm Millipore membrane cell. The membrane was then checked with helium to confirm a tight seal and that the membrane was defect (pinhole) free. Subsequently, the membrane was heated to operating temperature to begin permeation testing.

Figure 2. 25 mm Millipore membrane cell with high temperature Grafoil valve packing material used in place of a polymer o-ring. Maximum use temperature of Grafoil material is 650°C.

A special permeation measurement apparatus was constructed at CSM for the specific purpose of evaluating specialized membranes. Experiments to determine the pressure dependence of the H_2 flux were also performed at CSM. A new permeation cell for the 25 mm membranes was designed and fabricated. This cell was a scaled-down version of the one used for the 47 mm membranes. CSM encountered some difficulties with sealing the smaller 25 mm cells purchased from Millipore with the Grafoil valve packing material. The new cell is shown below in Figure 3.

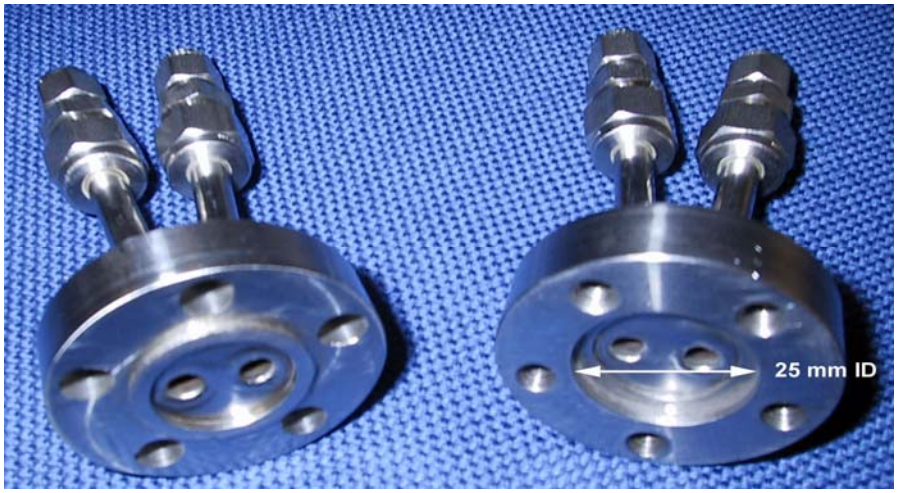

Figure 3. New stainless steel flow cell for 25 mm diameter membrane samples

A new test apparatus was plumbed and able to run two membranes at a time. As shown in Figure 4, two test cells can be simultaneously pressurized with the outlet flow independently determined from separate back pressure regulators. There were continued difficulties with the ceramic paper used to support the membrane and prevent damage when compressed between the graphite sealing gasket and the stainless steel support. Small punctures in the membranes were observed when a pressure difference was applied. Attempts to coat ceramic paper samples with boron nitrite and zirconium oxide, in and effort to produce a lower surface roughness and minimize damage to the membrane were attempted. Some porous stainless steel support discs were also coated with zirconium oxide in an effort to eliminate the ceramic paper entirely.

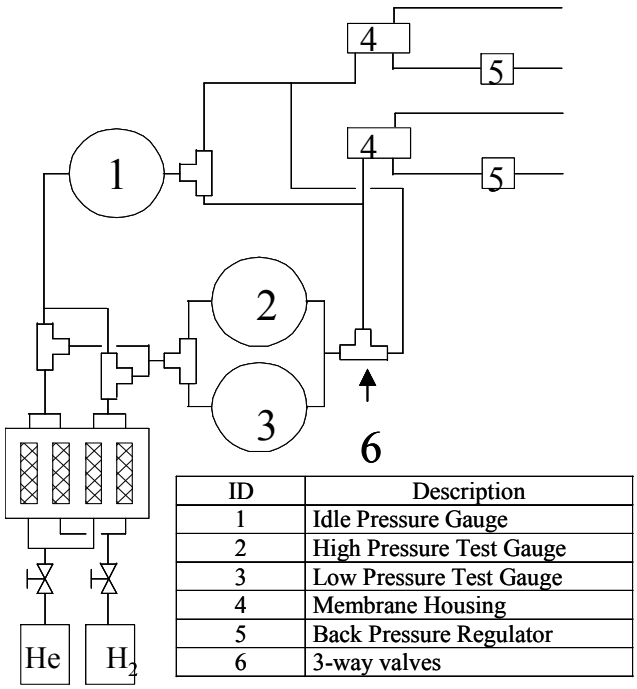

ID	Description
1	Idle Pressure Gauge
2	High Pressure Test Gauge
3	Low Pressure Test Gauge
4	Membrane Housing
5	Back Pressure Regulator
6	3-way valves

Figure 4. Schematic of CSM dual-cell permeation test system

Above and beyond the characterization of fundamental membrane properties, a key element of the effort was the participation of a leading-edge manufacturer of hydrogen purification equipment. Membranes were assembled into modules and tested at IdaTech. IdaTech has an extensive baseline of performance data for state-of-the-art Pd-alloy membranes and along with this experience in design and construction of specialized membrane support materials, was particularly well suited to both evaluate the SwRI produced membranes and make use of it in stand-alone purifiers as well as complete fuel cell systems.

RESULTS AND DISCUSSION

The project consisted of the three areas of membrane fabrication, testing/characterization and module construction and testing. The membrane fabrication was composed of development onto flexible and rigid substrates which involved specific technologies and activities. The results of each of these areas will be presented and discussed separately.

Vacuum Deposition – flexible substrates

Initially, a number of pure copper films were vacuum deposited on polyvinyl alcohol (PVA) and polystyrene substrates in order to optimize processing parameters using just e-beam evaporation alone and e-beam evaporation with ion assist. An example of a 3 micron-thick film on PVA is shown in Figure 5.

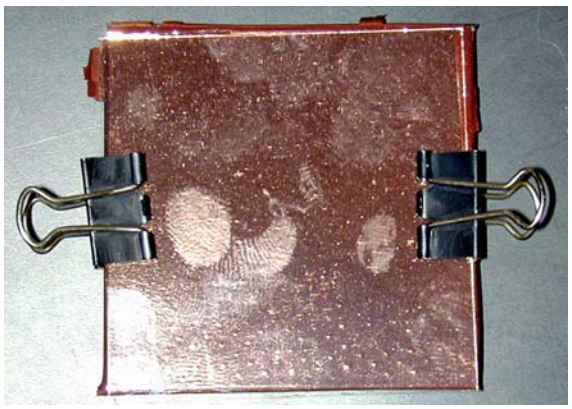

Figure 5. Copper film (3 µm) on PVA; sample is sandwiched between two pieces of glass

Pure copper and copper-palladium alloy films were deposited onto polyvinyl alcohol and polystyrene substrates (1-3.5 mils thickness) that were affixed onto both flat and curved metal backing plates; the backing plates were not actively cooled or heated. A set of experiments were conducted, adjusting various deposition processing parameters, in order to optimize film properties, i.e., minimal strain, defects, and composition, as a function of thickness (1-8 microns nominal thickness). An ion assist was used in conjunction with e-beam evaporation in order to control density and film stress.

Visually, the films were pinhole free although when the films were backlit, a number of submicron-sized pinholes were observed. These types of defects originate from essentially three sources: 1) particles/contaminants indigenous to the plastic substrate (either derived from processing or storage in an ambient environment), 2) airborne particles and background contaminants residing within the deposition chamber that are subsequently activated prior to, as well as, during deposition, and 3) micro-arcing of the e-beam source during the deposition process; the first two sources being a function of the electrostatic charge at the substrate (plastic) surface.

To better quantify these effects, a number of samples using different surface preparation techniques were prepared in addition to adding a surface "pre-cleaning" step in the vacuum chamber prior to deposition. All samples were prepared in a laminar flow bench, and transported from the hood to the chamber within a 'destat' plastic bag to minimize possible contamination from the background environment.

The as-deposited copper foil on untreated, 3.5 mil polystyrene film is shown in Figure 6; it is important to note that the backlighting technique to highlight the pinholes, actually enhance the size of a pinhole in the image, i.e., these microscopic pinholes are not detectable with the unaided eye. This level of defects would be considered representative of a coating on essentially any as-received plastic substrate. When rinsed or washed (without any abrasive action) with methanol prior to deposition, the number and type of defects drops dramatically as shown in Figure 7. Subsequently, combining a methanol 'scrub' with a methanol rinse slightly decreased the level of defects even further as shown in Figure 8.

Figure 6. 4 µm thick Cu film on un-treated, 3.5 mil polystyrene

Figure 7. 4 µm thick Cu film on 3.5 mil polystyrene, rinsed in methanol

Figure 8. 4 µm-thick Cu film on 3.5 mil polystyrene, scrub and rinsed in methanol

Figure 9. 4 µm-thick Cu film on 4 mil polystyrene, scrub and rinse in methanol

The level of defects shown in Figure 8 is analogous to those observed on an untreated glass slide and a glass slide wiped and cleaned in methanol. Hence, this level of defect density could be representative of the background particulate level within the chamber and to a lesser extent, micro-arcing from the e-beam source. A representative defect pinhole density for a 4 µm-thick Cu film on 4 mil polystyrene (gloss finish) is shown in Figure 9. Just as in the case of a Cu film on the 3.5 mil (matte) polystyrene film, a Cu film on the 4.0 mil (gloss) polystyrene film that has been 'scrubbed' and rinsed exhibits a similar defect pinhole density.

Cu films were also deposited on 2 mil PVA material; the PVA had been rinsed with isopropyl alcohol prior to deposition. The defect pinhole density is much less for this type of material and although it may not be reduced to zero, it certainly was reduced to a very low level. Other pre-treatment methods, such as plasma discharge, ionization, and surface pre-wetting were investigated to minimize defects during deposition and certain post-processing methods were also being investigated to create a gas impermeable membrane. Un-supported, strain-free films were produced at thicknesses less than 0.5 microns.

Having successfully produced pure copper films, processing parameters for co-evaporation of palladium-copper alloy films on both polystyrene and PVA substrates were established. Various deposition configurations were investigated in order to optimize film uniformity and reproducibility. Co-evaporated alloy films, from 20%Cu/80%Pd to 80%Cu/20%Pd were prepared. Examples of ~60%Pd/40%Cu alloy films (3 microns thick) on polystyrene and polyvinyl alcohol substrates are shown in Figure 10 (a) and (b) respectively. In addition to co-evaporated films, alternating layers of palladium and copper were produced to form multi-layer stacks of palladium-copper alloys. Pd-Cu alloy films were also fabricated using magnetron sputtering from a 60%Pd/40%Cu alloy target.

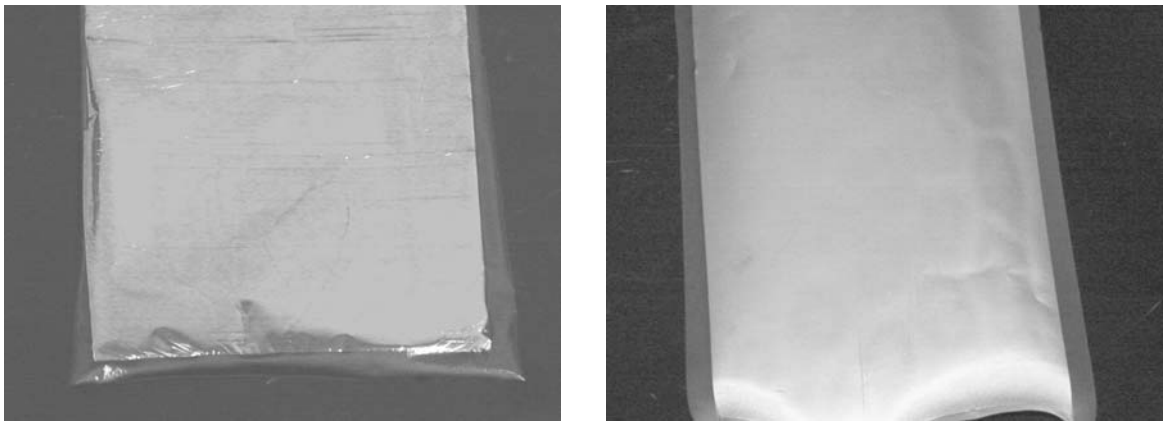

a) b)

Figure 10. Pd-Cu alloy films on a) polystyrene and b) polyvinyl alcohol films

Both pure copper and palladium-copper alloy films were successfully deposited onto polymer backing materials and subsequently removed via immersion in a low temperature solvent bath. Preliminary trials with co-evaporation and sequential evaporation of palladium and copper metals provided a better understanding of the challenges in producing a reproducible and uniform alloy composition. Although free-standing films, up to 6" x 8" in area at less than 0.5 microns in thickness, were produced, the process of developing techniques to minimize defect formation over large areas was required.

Additional Pd-Cu alloy films were deposited onto both PVA (Solublon) and polystyrene backing materials using magnetron sputtering and e-beam evaporation. In the case of magnetron sputtering, Pd-Cu films were deposited from a Pd-Cu target onto a plastic backing material in a batch, planetary configuration; whereas, in the case of evaporation, Pd-Cu alloy films were deposited onto plastic backing materials in a drum (web) coating configuration. A design of experiments (DOE) approach was implemented in the case of the evaporation experiments in the web coater to better evaluate the large number of parameters; i.e., metal deposition rates (1 – 4 nm/sec), web speed (0-0.2 m/sec), drum temperature, (0-60°C), plastic backing film (Solublon, polystyrene), and others.

The Pd-Cu alloy films were formed on polymer backing materials in the 12" wide drum or web-coating system schematically illustrated in Figure 11. Deposition rates of palladium and copper were independently controlled using crystal quartz monitor and electron impact emission spectroscopy (EIES). After having established uniformity profiles and elemental distribution across the deposition zone, the DOE was conducted to correlate processing parameters (i.e., deposition/web feed rates, drum temperature, polymer pre-treatment, etc.) with final properties (response) of the Pd-Cu alloy films (i.e., composition, defects, strain). From the initial DOE tests conducted on PVA (Solublon), we observed excessive film strain and corresponding delamination at total deposition rates greater than 2 nm/sec and for web feed rates <0.001 m/sec. The goal for the initial trails was to define rates such that Pd-Cu alloy films could be produced with minimal defects and strain. Since total thickness of the films were kept low (<250 nm) in order to rapidly screen processing conditions, the resulting films were too thin to remove the backing polymer material.

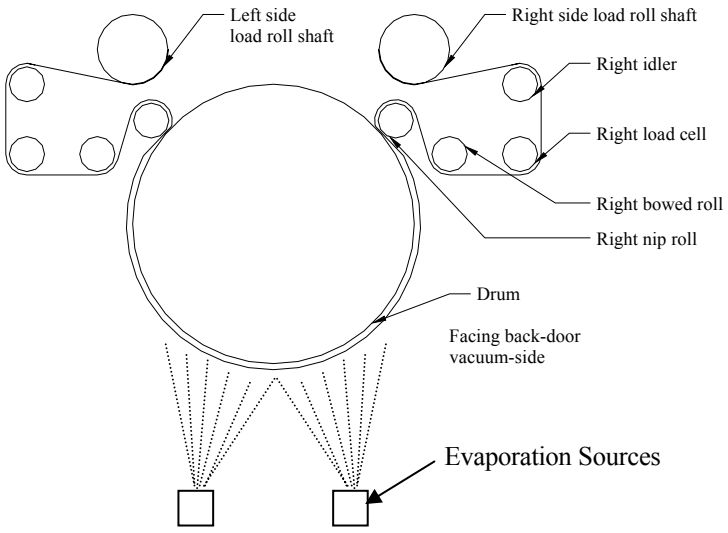

Figure 11. Schematic of web roll coater with evaporation sources

Pd-Cu alloy films up to 5 x 5" in area (1-3 microns thick) were created using both magnetron sputtering and e-beam evaporation on PVA (Solublon) and polystyrene backing materials. A set of experiments were also conducted to assess processing methods/solutions chemistry for removing the polymer backing material from the Pd-Cu film. Using two Cu films (10 micron thickness total) in a sandwich configuration, leak rates were measured to be about 20% of the background leak rate.

Using the procedures outlined in the experimental section, a number of metal films were successfully removed from the polymer backing material (both PVA (Solublon) and polystyrene) and retained on the porous Monel grid material. The Pd-Cu alloy coated plastic samples were first cut into discs 75 mm in diameter, sandwiched together with a porous metal disc (Monel) between two microscreens and then clamped (refer to schematic in Figure 12). To remove the plastic backing material, the samples are then lowered horizontally, coated polymer discs up, Monel mesh down, into the appropriate solvent; hot water (60- 80°C) for Solublon and chloroform (room temperature) for polystyrene. Polymer dissolution (removal rate) was evaluated as a function of temperature and time. Nominal times were 30 seconds for the Solublon and 600 seconds for the polystyrene. Upon dissolution of the polymer backing material, samples were removed from the solvent, carefully disassembled and then dried.

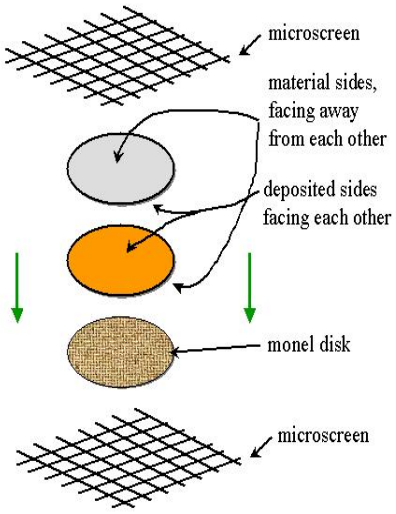

Figure 12. Schematic of sandwich configuration

Both polystyrene and PVA (Solublon) represent unique challenges in the development of procedures for removing or separating the Pd-Cu film from the plastic. A first order effect on the properties of the final Pd-Cu alloy film was the intrinsic strain or stress in the film. At the one extreme, too much stress in the film lead to total fragmentation of the thin film as the supporting polymer material was dissolved away. Extrinsic stress formed due to thermal expansion differences between the metal and polymer. For example, a fully dense, contiguous metal layer (i.e., wetting) at the polymer surface is less compliant and with the thermal expansion differences between the metal film and the polymer backing material, excessive strain built up in the film and promoted fragmentation in the backing removal process.

Building upon the preliminary results a series of tests using both magnetron sputtering and e-beam evaporation in the drum web coating system were completed. In the case of magnetron sputtering from a 60% Pd, 40% Cu alloy target, films were produced on 25 cm-wide PS and PVA material up to ~2 meter lengths. Although adherent films were produced with very low strain, the films did not remain intact upon release from the backing material; i.e., films disintegrated into small fragments with the Pd-Cu alloy films on polystrene forming much larger fragments than those on PVA. The fragmentation can be explained by the non-optimized plasma treatment of the plastic surface (functionalization) to increase the surface energy. Also, the observed differences between the PVA and PS was attributed to the amount of adsorbed water; i.e., the higher level on PVA creating a more non-wettable surface.

In the case of e-beam evaporated films, the formation of contiguous alloy layers at deposition rates greater than 5 nm/sec was found to be difficult. Pure Cu and pure Pd single layer films were produced in the web coater to demonstrate formation of 25 cm-wide, contiguous film.

All Pd-Cu alloy films on plastic contained some level of defects (pinholes) and until the pre-treatment conditions were optimized to properly functionalize the surface, these types of defects remained. Significant effort was placed on developing processing procedures for the formation of 1-5 mm-thick, Pd-Cu alloy films on PVA and PS backing materials. Pd-Cu alloy films, up to 25 cm widths were produced although due to non-optimal pre-treatment of the polymer surface, films were either not contiguous or fell apart during the backing removal process or contained some level of defects.

As part of the effort to reduce through-thickness defects in as-deposited membranes less than 5 μm, techniques were investigated to modify and optimize the surface properties of the sacrificial polymer backing material(s). Since surface energy and roughness of the polymer surface can have a dramatic effect on the agglomeration and wetting characteristics of a vapor deposited film, two approaches were selected to optimize surface properties of the polymer, 1) in addition to PS and PVA (Solublon), testing of other polymers, such as Kapton (polyimide), and PET were included to expand the range of polymer surface energy, and 2) surface pretreatment (modification) with argon (Ar)/oxygen (O) (95/5) plasma (Ar to create long-lived carbon radicals and O to create functional groups, such as hydroxyl, carbonyl, or carboxyl).

Both patches and continuous segments (11" wide and up to 48" in length) of the polymer films were treated/coated in the vacuum web coater (controlled drum temperatures between 0-60^{o}C) using either co-evaporation of Pd and Cu or magnetron sputtering from a composite target. Plasma treatments were conducted in-line with the Pd-Cu deposition steps.

Although procedures were developed and routinely employed to deposit and release Pd-Cu films, 2-5 μm-thick and >75 in^2 in area from PS and PVA polymer backing materials through-thickness defects (pinholes) for film thicknesses less than 6 μm were significant. Though a small percentage of the defects were related to the deposition process (and therefore potentially eliminated), the majority of defect were due to characteristics of the sacrificial substrate.

In the case of flexible polymer substrates, the low surface energy (related to surface functional groups), roughness, and surface charge (electrostatic) promoted defect formation by methods such as surface particles/contamination, or agglomeration/clustering of incident atoms (as opposed to spreading (wetting) into a contiguous layer). Whether a particle or a cluster on the surface, at some point in the deposition, the incident atoms must bridge across these points to form a contiguous film. Although this "abridged" film is essentially contiguous, the coating contained "through-thickness" defects (porosity) that compromised the mechanical integrity of the film; i.e., with only minor tensile stress, the reduced cross-section induced at the defect broke and formed a pinhole. Hence, to form a <5 μm-thick, free-standing, gas impermeable membrane, the characteristics of the substrate must be such that vacuum deposited films must spread at thicknesses much less than 1μm.

Two treatments methods were investigated to promote spreading of the Pd-Cu films on the polymer backing materials; i.e. Ar/O_2 plasma and deposition of a precursor layer, such as SiO_x with a more favorable surface energy. Although argon plasma treatment (with 5% O_2) was shown to decrease water contact angles (increase film wettability) on all plastics tested (PS, PVA, Kapton, and PET), defects in films less than 5 μm remained. Subsequently, based on results on rigid silicon substrates, an

evaporated silica (SiO_x) layer was deposited on plasma treated polymer substrates. Unlike the case for rigid silicon substrates, the SiOx-coated polymer substrates did not yield films with a lower defect density. Therefore, irrespective of the surface treatment options tested (plasma or seed layer), defect-free Pd-Cu films on flexible polymer substrates over large areas at thicknesses <5μm could not be produced. It is important to note however that defect-free films were produced at thicknesses >6 μm.

Vacuum Deposition – Rigid Substrates

As an alternative to address the issue of defects in the Pd-Cu alloy membrane on flexible substrates, films were deposited onto smooth, thermally oxidized silicon wafers. The reasoning was that particulate and other contaminants can be more readily controlled (i.e., minimized) on a silicon surface in comparison to plastic, and is considerably smoother than plastic. In preliminary experiments using magnetron sputtering, a relatively pinhole-free coating was produced that easily released from the silicon substrate (poor adherence). In general, the key factors that affect formation of a thin, dense, defect-free, Pd-Cu alloy film are surface energy, roughness, and oxygen/moisture content of the backing material. By using thermally oxidized silicon wafers, the surface roughness was reduced while at the same time, controlling surface chemistry, and more specifically, oxygen activity. Correspondingly, using vacuum processing conditions that have been optimized to minimize intrinsic film stress, pinhole-free Pd-Cu alloy films at thicknesses between 6 – 12 μm were produced. Discs, 1" in diameter, were cut from the released Pd-Cu films on silicon and then tested for H_2 permeation (a photograph of the Pd-Cu alloy foil after removal of discs, is shown in Figure 13).

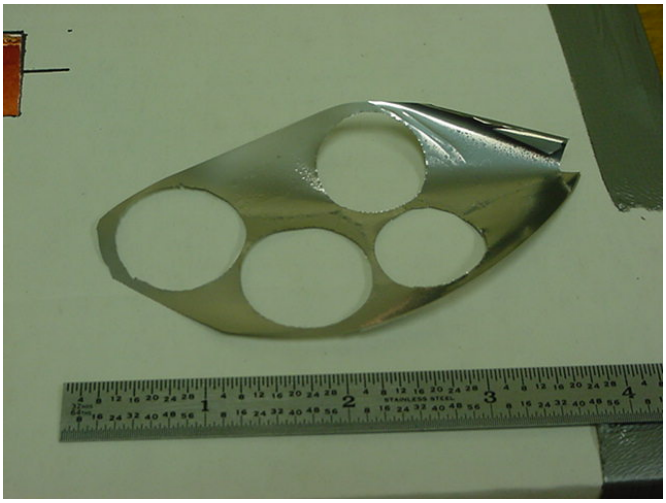

Figure 13. As-fabricated, 12 μm-thick Pd-Cu alloy film, released from thermally oxidized silicon wafer substrate, showing 1"-diameter cut-outs for H_2 permeation measurements

Since the primary cause of through-thickness defect formation in thin-films is due to surface particle contamination prior to deposition, methods established in the semiconductor industry, to minimize and essentially eliminate defects from particle contamination were utilized. Using rigid silicon and a glass slide, the effect of particle contamination (or lack thereof) on the formation of defects in the films less than 5 μm-thick was demonstrated. Using established vacuum deposition

parameters and surface pretreatments of silicon and glass that have enabled defect-free production of 5µm-thick Pd-Cu films on 4" diameter silicon and 4" square glass substrates. A released Pd-Cu film is shown in Figure 14 below.

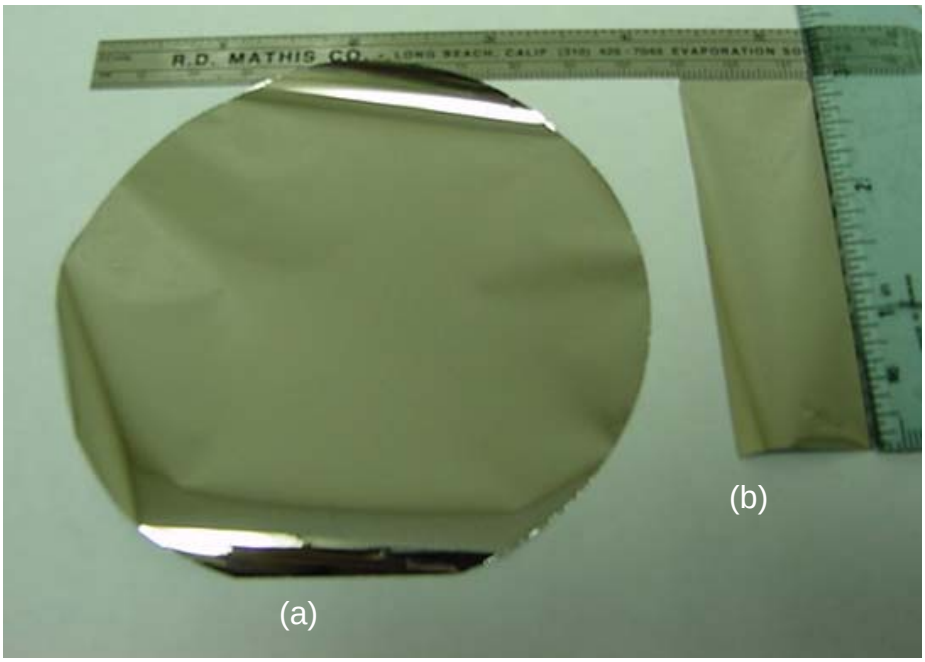

Figure 14. Free-standing Pd-Cu Foils, 5 µm-thick; a) from rigid, 4" silicon wafer and b) glass slide

A strong correlation between sputter deposition power and the formation of defects (pinholes) was observed; namely, the higher the power, the greater the probability of pinhole formation assuming everything else remained constant. However, optimum release did not always coincide with low power. Films less than 1 µm-thick were successfully released from both silicon and glass substrates although the minimum thickness for pinhole-free films over a 4-inch diameter disc was on the order of 3-4 µm.

Although processing parameters were established for releasing 5 µm-thick films from 4" diameter oxidized silicon and polished borosilicate glass, the long term goal was to produce thinner films with larger surface areas and with greater reproducibility. To accomplish this goal on a rigid backing substrate, procedures for releasing thinner films from inexpensive soda-lime glass were developed. Different types of pre-cleaning procedures (both wet chemical and dry vacuum ion sputtering), in addition to pre-deposition of a thin release layers such as 10 nm-thick Al_2O_3, were investigated on the soda-lime glass in order to achieve consistency in film release and mechanical properties. Although 2.5 µm-thick films were consistently deposited onto the supporting soda-lime glass substrates (up to 230 cm^2 in area) without defects (as determined with "back-lighting" methods), defects were created in the films during the process of releasing the films from the glass substrate. Defect formation during release was directly attributable to surface contamination and variability in the cleaning procedure.

Testing of three different types of rigid supporting substrates, thermally oxidized silicon (10 cm diameter), polished borosilicate glass (10 cm diameter), and soda-lime glass (>100 cm^2 areas) continued with each representing a different cost, surface roughness, and chemistry, with an overall goal to produce thinner (<4 μm-thick), defect-free Pd-Cu films over larger areas (>100 cm^2). Mechanical integrity, defect density, and release characteristics of the films, though similar for the oxidized silicon and borosilicate glass, were distinctly different for the inexpensive soda-lime (float) glass; i.e., more sensitive to surface impurities. In general, films less than 4 μm-thick were shown to be very sensitive to surface condition of the supporting substrate, particularly in the case of the soda-lime glass, to the point where surface strain overrode and dominated the intrinsic bulk stresses that are produced during the growth process. In thicker films (>5 μm), interface stresses are more adequately balanced by intrinsic bulk stresses such that the bulk stresses control the release characteristics. Since bulk stresses are controlled by the growth characteristics (processing parameters), overall release characteristics and film properties are more easily controlled in thicker films.

With the goal of understanding the release characteristics of the film, characterization of the interface between the glass substrate and the film following release was completed. In general, the side of the film that was in contact with the glass would re-adhere to the glass when placed in contact with the glass. This attraction was primarily observed on the side that was in direct contact with the glass substrate during deposition; i.e., the top surface of the film (away from the substrate) did not exhibit any attraction to the glass substrate. This "Velcro" type effect was observed whenever the released side of the film was placed in contact with any surface that had been previously used for film preparation (i.e., a glass surface or even another metal surface). There appeared to be a type of key-lock type of relationship between the released surfaces.

The released metal surfaces were analyzed with Auger Electron Spectroscopy (AES) to check for trace elements and, other than the typical carbon and oxygen, no other trace elements, such as silicon were detected. The "released" surface, as shown in the SEM image in Figure 15(a), was essentially featureless at the magnification shown although the top surface (Figure 15) exhibited some degree of texture (from profile measurements, the surface roughness was estimated to be less than 3 nm).

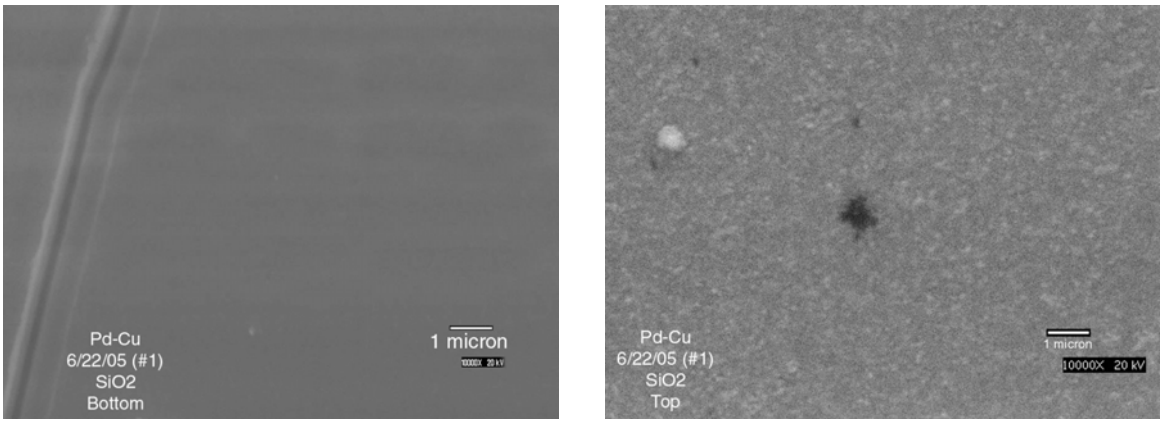

a) b)

Figure 15. SEM image of Pd-Cu film at the a) release surface and b) top surface; films grown on (and released) from polished borosilicate glass.

Having previously established procedures for depositing a Pd-Cu film, with varying thickness and compositions, on a variety of substrates over large areas, the focus shifted to developing procedures for producing pinhole-free, free-standing films at a thickness less than 5 μm and up to 6" diameter surfaces. To produce defect-free, pinhole-free coatings less than 5 μm in thickness, the presence of micron and even sub-micron-size particulates had to be minimized or through-thickness pinholes in the film membrane would develop. Although particulates can be essentially eliminated in a clean room environment, the goal for this program was to utilize methods and procedures that do not require a class 10 or better rating.

Procedures were therefore established to clean the substrate prior to loading in the deposition chamber. Both oxidized silicon (6" diameter) and polished silica (4" diameter) substrates were coated with Pd-Cu. First, the substrates were given a careful visual inspection and any visible particulates were removed using optical-grade wipes. Next, the samples were dusted off using an Ion-Air Model 7901 de-ionizing gun fed by ultrahigh purity nitrogen. This removed any remaining particulates that were electrostatically bound to the surface. The substrates were then mounted face down in the vacuum chamber and prior to sputter deposition, a radiofrequency (RF) plasma cleaning procedure was developed with the goal of removing surface contaminants and "functionalizing" the surface to enable the proper adhesion and release characteristics. The RF clean was subsequently shown to reduce surface contaminants (including particulates) and resulted in the production of pinhole-free, 3 μm thick films.

At the beginning of the deposition, processing conditions were established to create a thin, <100 nm compliant layer for stress control and film release. The use of oblique angle and/or high pressure deposition conditions during magnetron sputtering are known to create porous/near amorphous structures that are compliant and therefore, this approach was incorporated into the film growth procedures. An SEM cross section of a 3 μm, Pd-Cu film is shown in Figure 16 where the 60 nm compliant layer can be seen at the bottom (released) surface of the film and a fine-grained, columnar structure is observed throughout the bulk of the film section.

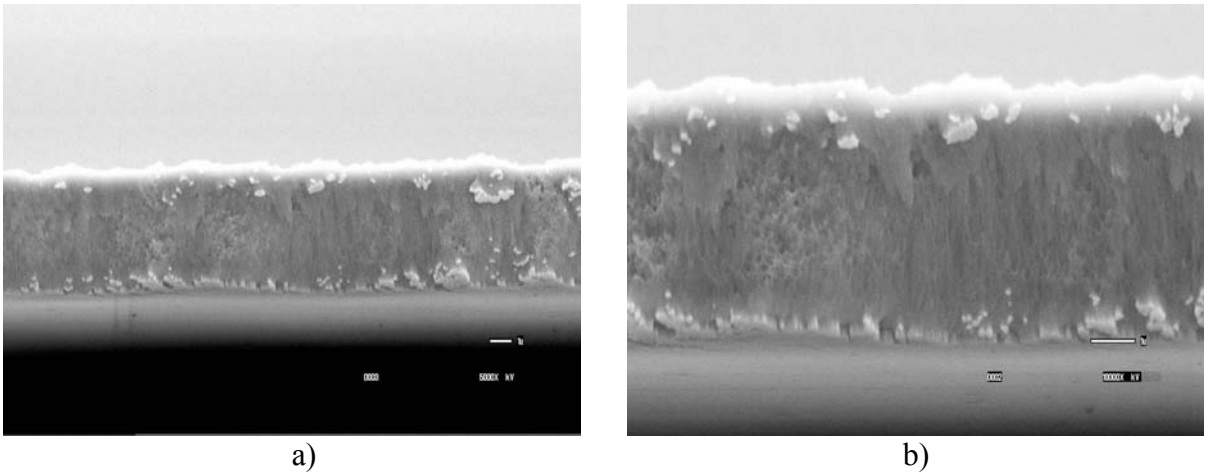

a) b)

Figure 16. Cross section of magnetron sputtered, Pd-Cu film with 60 nm compliant layer at (a) 5000X and (b) 10000X magnification.

A top view of the film presented in Figure 16 is presented in Figure 17 below. A number of these films, 6" in diameter and 3 μm thick, were prepared with essentially neutral stress in the as-deposited condition. The films release consistently, without damage, and with minimal adhesion to the substrate; it is important to note that this adhesion could be adjusted to obtain ideal release parameters.

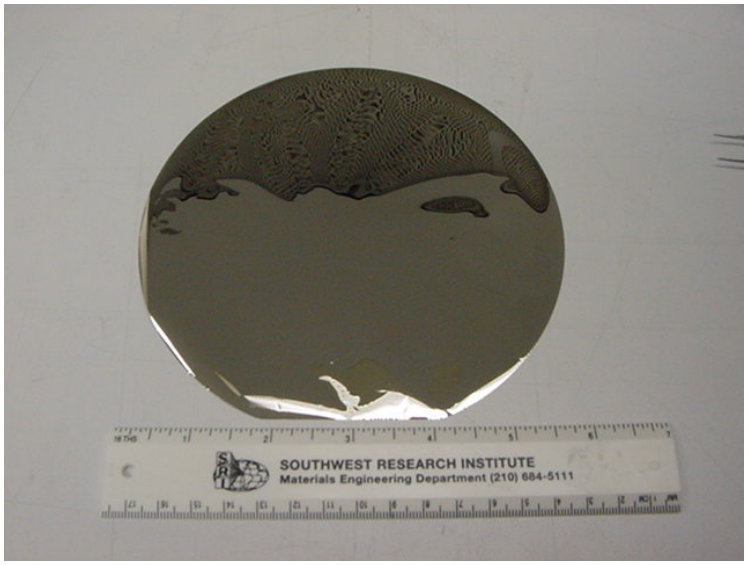

Figure 17. As-deposited (and released), 3 μm -thick, 6" diameter, Pd(60)-Cu(40), film (grown on oxidized silicon wafer).

New procedures were developed and implemented to improve reliability and repeatability of release characteristics from the temporary substrate (i.e., silicon wafer) and to minimize through-thickness defects in a 6" diameter film, 3 microns in thickness. With the new procedures, stress free films, with zero or minimal defects (less than 5) across a 6" diameter area were consistently produced (It is important to note that for those films containing pinholes, a procedure was developed to repair the pinholes to form a gas tight seal). The films were all within the identified tolerance range for composition (i.e., 60 +/- 0.2 % Pd). Approximately ten 6" diameter samples were shipped to IdaTech for evaluation and testing in a small module configuration. This represented a significant internal milestone for the project.

A 4-factor, 16-run series of experiments was conducted to examine the effects of pre-cleaning conditions and compliant layer deposition on the stress, release, and defect density of Pd-Cu films deposited to a nominal thickness of 5 μm on 4-inch diameter silicon wafers. The experimental design is summarized in Table 2. Two different radio frequency plasma cleaning power settings and times were selected in addition to two different compliant layer deposition times (proportional to compliant layer thickness) and pressure. The hypothesis was that the cleaning conditions might affect the release characteristics and pinhole density of the membrane while the compliant layer could influence the membrane intrinsic stress as well as release. In all cases, the base vacuum pressure ($7x10^{-7}$ Torr), membrane deposition conditions (500W at $8x10^{-4}$ Torr), and thickness (3 μm) were fixed.

Table 2. Four factor design of experiments

Run #	Plasma Cln Time (min)	Plasma Cln Power (watts)	Compl Layer Time (min)	Compl Layer Press (mTorr)
1	15	18	1.5	10
2	15	18	1.5	24
3	15	18	3	10
4	15	18	3	24
5	15	38	1.5	10
6	15	38	1.5	24
7	15	38	3	10
8	15	38	3	24
9	45	18	1.5	10
10	45	18	1.5	24
11	45	18	3	10
12	45	18	3	24
13	45	38	1.5	10
14	45	38	1.5	24
15	45	38	3	10
16	45	38	3	24

Evaluation of the membranes produced in the design of experiments yielded the following information summarized in Table 3. All membranes released completely from the silicon wafer backing regardless of the process conditions. The number of defects varied considerably from 6-150 defects per sample but no statistically significant correlation could be established between the number of defects and any of the process parameters. For membrane stress, the compliant layer deposition time (related to compliant layer thickness) was correlated with statistical significance. In general, the thicker the compliant layer the more tensile stress was developed in the membrane.

Table 3. Measured number of pinhole defects, % release, and membrane stress measured for each trial

Run #	# of Defects	% Release	Relative Stress
1	15	100	0
2	23	100	3
3	7	100	-3
4	8	100	-1
5	15	100	0
6	16	100	5
7	6	100	-3
8	7	100	-2
9	9	100	-1
10	6	100	0
11	23	100	-5
12	14	100	-3
13	14	100	5
14	29	100	1
15	150	100	-5
16	16	100	5

Based on the results of these trials, optimal deposition conditions were selected and adapted for use in the preparation of membranes on 12-inch diameter silicon substrates. A new RF plasma cleaning apparatus was constructed to accommodate the larger samples and different methods for rotation and translation of the substrate with respect to the Pd-Cu sputter target were investigated in an effort to optimize the thickness uniformity and stress across the membrane. Figure 18 shows a Pd-Cu membrane, approximately 3-4 microns thick, prior to its release from the substrate. The chevron pattern is simply a reflection off the filter grating of the laminar flow bench where the photo was taken. While some cracking developed in the membrane as it released at the edges of the wafer, several large sheets of membrane material with near-zero internal stress were harvested for testing. Pinhole densities numbered fewer than 10 across the entire wafer in at least one instance. A small number of 2" by 8" membranes were carefully cut using a simple quilting knife (similar to a pizza cutter) with one finished example shown in Figure 189. Two samples were provided to IdaTech for incorporation into a new module design.

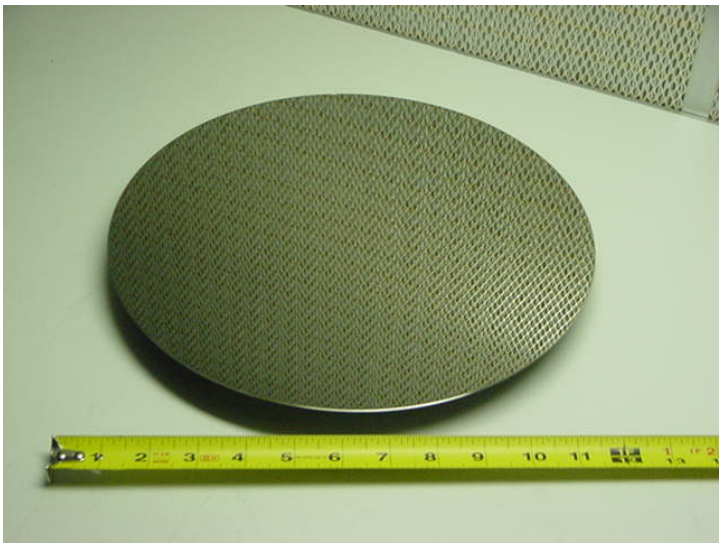

Figure 18. Pd-Cu membrane deposited on 12-inch silicon wafer

Figure 19. Rectangular membrane cut from 12-inch sample

A dozen large membranes were produced with as few as six pinholes found over the entire membrane. Figure 20 shows one of these specimens laid flat on a sheet of glass. In general, the pinholes were largely confined to the edges of the membrane. As part of the preparing 2" x 8" membranes for IdaTech, selected membranes were cross-sectioned and the thickness measured at 1-inch intervals across the diameter of the sample using a stylus profilometer.

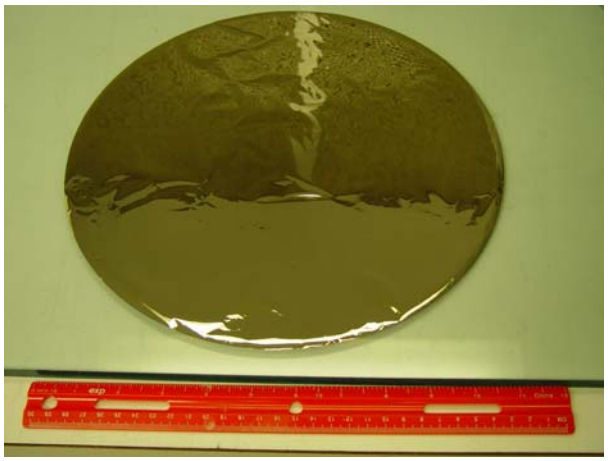

Figure 20. 12-inch low stress Pd-Cu membrane approximately 4 microns thick

Figure 21 is a graph of thickness as a function of position across the diameter of a representative 12-inch Pd-Cu membrane. As the membrane material built up on the silicon support, the sample was rotated and translated across the Pd-Cu sputter target. The average thickness of this membrane was 5.3 microns with a thickness variation of approximately 20%. By using a larger sputter target or a different rotation/translation pattern, the thickness variation could be reduced to less than 5%.

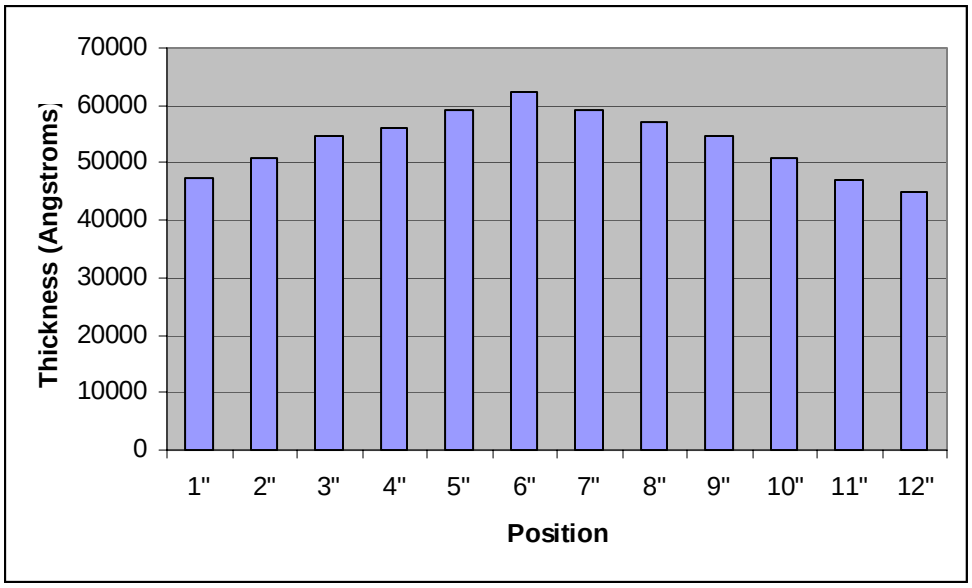

Figure 21. Measured thickness as a function of position across the diameter of a 12-inch PdCu membrane.

In order to provide IdaTech with a sufficient inventory of membranes for use in their test assemblies, additional deposition runs were carried out on 12-inch diameter silicon wafers. One important finding was that after the membrane was deposited and removed, the wafers could be reused to make additional membranes with minimal additional pinhole defects if the substrate was properly cleaned.

Another study initiated with CSM was an effort so examine the permeability of vacuum fabricated membranes as a function of Pd content. Specifically, the objective was to determine if the structure of these membrane differed from conventional rolled material as a function of Pd-Cu stoichiometry. To achieve these compositions, additional small pieces of pure Pd were placed on top of a nominal 60-40 Pd-Cu sputter target. After a tooling run was conducted, the composition was measured by EDS and adjusted by placing additional pieces or repositioning the pieces until the desired composition was obtained. Figure 22 shows the target with several pieces of Pd added in an effort to create a Pd content of ~66%. Membranes with 62-66% of Pd were produced and samples shipped to CSM.

Figure 22. Sputter target modified to increase the membrane Pd content

Some effort in this program was dedicated to the preparation of ternary alloy membranes. Work by Kamakoti and Sholl at Carnegie Mellon University using density functional theory to model the hydrogen transport through a membrane has suggested that alloy additions of 3-5 wt% of Rh, Ru, and possibly Ta could have a significant impact on the hydrogen binding and activation energies in Pd-Cu alloys. In an effort to experimentally validate some of these predictions, small pieces of 99.9% pure Ru, Rh, and Ta were placed at different locations of the Pd-Cu sputter target. Silicon witness samples were coated with 0.5-1.0 micron layers in short "tooling" runs and analyzed using EDS to determine the composition. By adding or removing some of the Rh, Ru, or Ta pieces from the sputter target, the desired stoichiometry could be obtained. The EDS composition measurements for three representative ternary alloy membranes are shown in Table 4. Magnetron sputtering is uniquely suited for the rapid preparation and screening of new ternary alloys because the composition can be quickly changed simply by tiling different areas of material on the target.

Table 4. EDX measurements of PdCuX ternary alloy membranes

Run #	Pd wt%	Cu wt%	X %
022106#1	56.6	37.5	5.9 Ru
030706#1	57.7	37.5	4.8 Ta
031406#1	54.4	38.4	7.2 Rh

The release characteristics of Ru and Rh doped Pd-Cu membranes was quite similar to the binary alloys while the Ta alloy strongly adhered to the silicon backing. This problem was overcome by depositing a thin layer of pure Ta from a separate sputter source between two thicker layers of Pd-Cu. The sample was annealed before testing to diffuse the Ta throughout the membrane. A number of 1-inch and 2-inch square membranes of each alloy composition were provided to CSM for evaluation. Several small membrane samples were provided to Dr. Steven Paglieri at Los Alamos National Laboratory for independent testing and evaluation.

As-deposited membranes are usually an in the fcc phase and transform to bcc or mixed fcc+bcc upon heating to 400°C. Because the membranes were very thin it was postulated that it might not be possible to assemble the membranes into a module while still in the fcc phase as the change in lattice parameter associated with the phase transformation could result in a slight contraction that could place significant stress on the membrane and cause it to rupture. Hence a series of annealing experiments were conducted to convert the membrane to the desired phase prior to assembly in a module. Figure 23 shows the arrangement developed to hold the membranes during annealing. The membrane was held between two pyrex glass plates held together with simple binder clips which were stripped of paint prior to use. Stainless steel lock wire was used to maintain a separation between the plates to limit air entrapment and allow to membranes to expand or contract more freely without curling. After mounting, the membrane samples were placed in a tube furnace purged with a continuous flow of Ar and annealed at 450°C for 12 hours.

Figure 23. Photograph of fixture used to hold membranes flat during annealing

The performance of these annealed films will be discussed in the following sections.

Test/Characterization

Preliminary Gas (He) Leak Testing

A system was put together quickly to characterize the leak rate of the metal film samples sent to CSM at room temperature. A schematic of the simple leak test apparatus is given in Figure 24 below.

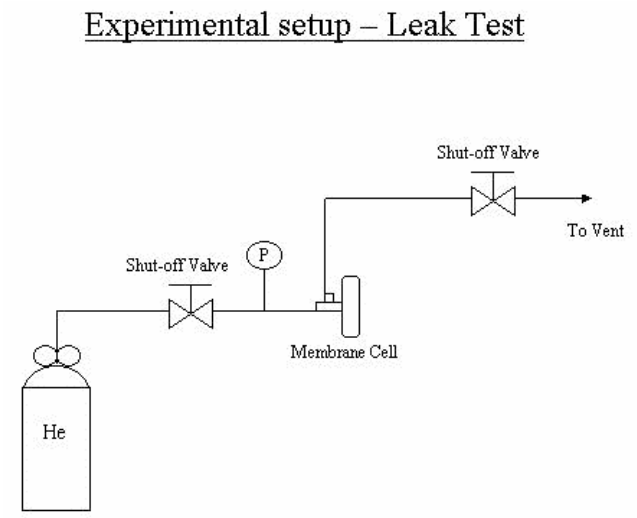

Figure 24. Schematic of CSM inert gas leak test apparatus

The heart of the apparatus is a 25 mm diameter, stainless steel membrane holder manufactured by Millipore. The test procedure was to pressurize the feed side of the membrane cell to a moderate pressure, 50 – 100 psig, and then measure the time necessary for the feed pressure to decay. A simple material balance expression is used to estimate the leak rate of the sample gas, which was then normalized by the membrane area (19 mm diameter area available for permeation = 2.8 cm^2 = $2.8 \bullet 10^{-4}$ m^2). A baseline leak test was run on the apparatus using a relatively thick Al foil sample, assumed to be leak free. This test was to ascertain the leaks in the plumbing and the o-ring seal in

the Millipore membrane holder. The baseline leak rate, using He, was $3 \cdot 10^{-8}$ mole/s with the Al foil in the cell. The baseline leak is then subtracted from the He leak rate of the samples.

As per the procedures outlined in the experimental section, the leak rate of the metal foils were characterized. The original single metal films contained defects across a 25 mm area, two films were sandwiched together in order to evaluate the leak test apparatus. Sample films exhibited leak rates between five times the background He leak rate and 20% the background. For comparison, when composite Pd and Pd alloy membranes made by electroless plating were leak tested, the N_2 leak rate was typically $\leq 10^{-4}$ mole/m^2•s before annealing. Annealing at temperatures above 300°C typically reduced the leak rate further. Typical pure hydrogen fluxes for composite Pd alloy membranes of micron thickness were in the range of 0.1 – 0.5 mole/m^2•s for a 50 psig feed gas.

There were problems relating to film damage by the o-ring in the Millipore test cell. As shown in Figure 25, the force exerted on the film by the Viton o-ring pushed the thin metal film into the large pores of the Monel screen support to create a huge leak path. In addition to substituting alternative porous structures for support (i.e., ceramic and stainless steel sponge materials) as one approach to overcome the problem, swaging a thin foil, and/or re-flowing a braze alloy, such as Au-Si, into the pores of the Monel screen and in order to provide a smooth sealing surface were considered.

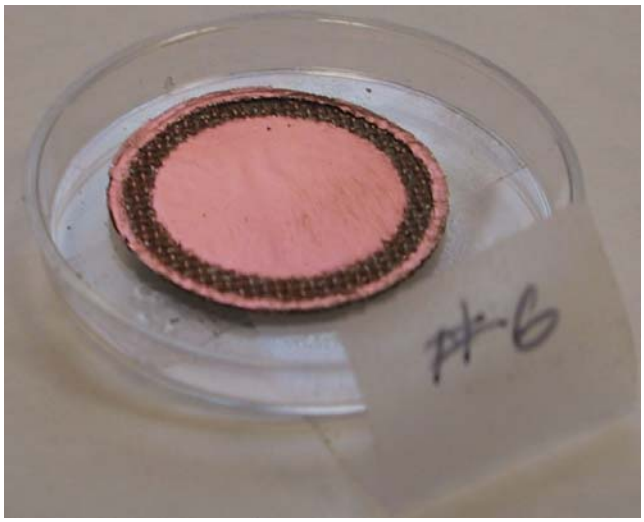

Figure 25. Damage to Cu film caused by pressure from o-ring seal

Permeation Testing

Permeation characteristics of a 25 μm-thick, $Pd_{60}Cu_{40}$ alloy foil from the Wilkinson Company were conducted. Prior to measuring the permeation characteristics, the foil was annealed under hydrogen for 5 days at 450°C to facilitate formation of the higher permeability, β -phase, followed by a 1-hour treatment in air at the same temperature. XRD analysis, before and after annealing, clearly indicated that the foil had changed from the a-phase to the b-phase. Pure H_2 permeation tests were carried out with a trans-membrane pressure between 15 and 50 psi, all at 400°C. Figure 26 shows a plot of pure gas permeability versus differential pressure raised to the one-half power. The H_2 permeability was determined to be 5.4 x 10-5 $cm^3 cm cm^{-2} s^{-1} cmHg^{-1/2}$. This is in good agreement with the Juda Patent (USP 6,238,645). See Figure 27.

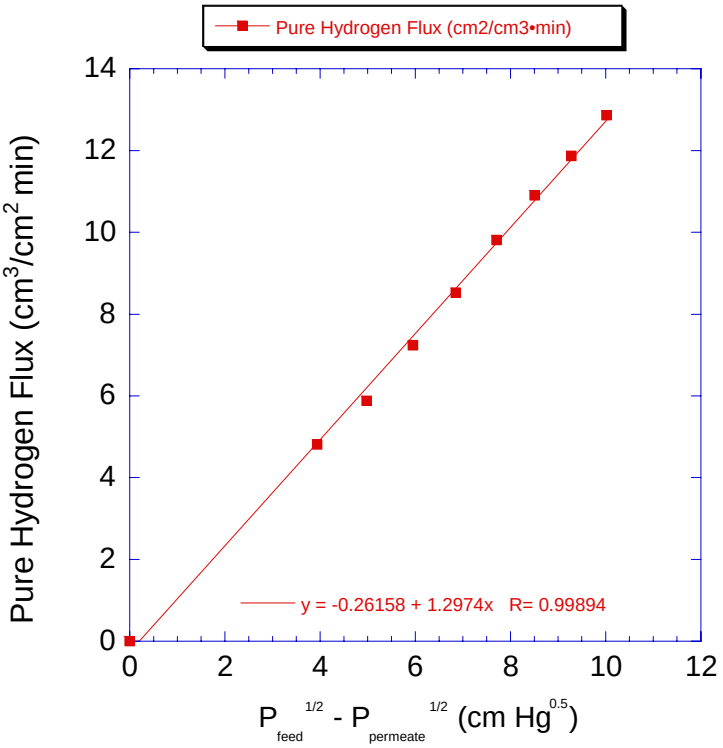

Figure 26 H_2 flux versus differential pressure of 25 µm thick $Pd_{60}Cu_{40}$ alloy foil at 400°C.

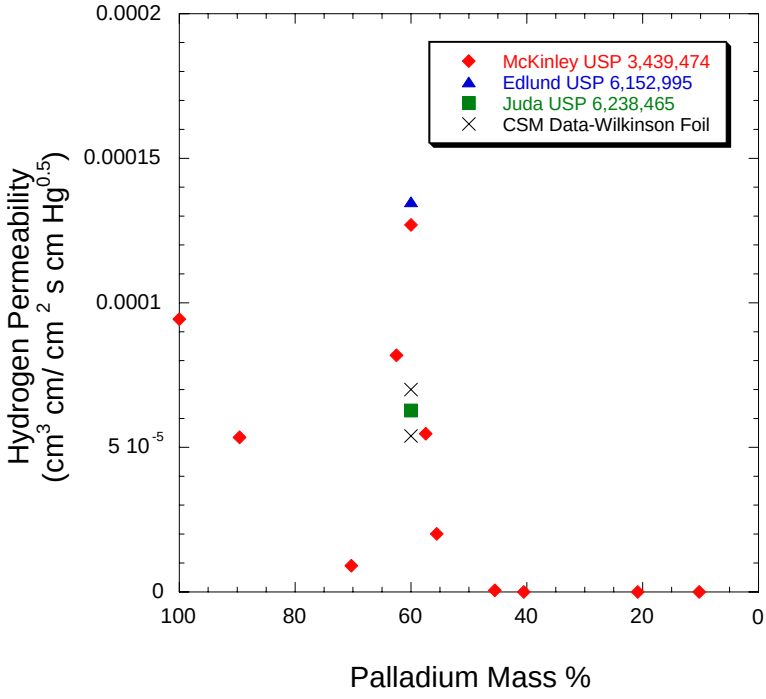

Figure 27. H_2 permeability of $Pd_{60}Cu_{40}$ foils in the patent literature at 400°C.

To insure mechanical integrity of the foil(s) at operating temperatures and pressures, the foils were supported by a porous plate (or mesh) material, typically metallic. Initially, the same Monel mesh material used in IdaTech's commercial hydrogen production system was adopted but due to the roughness of the mesh, it was not possible to form a leak-tight seal in the bench-scale, Millipore test apparatus. Therefore, a number of alternative porous support options were evaluated, such as porous stainless steel (Mott Metallurgical), porous Vycor glass (Corning), anodic porous aluminum (0.02 μm pore size from Whatman), aluminum paper (Zircar), and silver membranes (0.45 μm pore size from Millipore).

A control experiment was performed to investigate the effect of annealing and oxidizing the foil membranes prior to H_2 permeation experiments. A cleaned, but not annealed or oxidized, Pd-Cu foil membrane was installed in the permeation cell, heated to 400°C under inert gas and then tested under pure H_2. From prior experience, the H_2 flux was expected to increase slowly with time as the foil annealed and the bulk structure changed from fcc to bcc. However, the flux increased sharply to about 60% of the flux observed in prior experiments and then decreased with longer times. The temperature was increased to 500°C and an *in-situ* air purge was performed but the H_2 flux did not increase, and in fact decreased to essentially zero. The appearance of the metal foil was very different from those observed previously; possibly due to carbon contamination, pyrolysis of oils, introduced during fabrication of the foil. It is important to note that the foils were cleaned prior to treatment.

Permeation testing of another 25 micron thick, $Pd_{60}Cu_{40}$ foil membrane from the Wilkinson Company was repeated with a different membrane from the same lot of film. The H_2 permeability was determined to be $7.0 \bullet 10^{-5}$ $cm^3 \bullet cm/cm^2 \bullet s \bullet cm\ Hg^{-1/2}$. This permeability measurement was about 30% higher than the value initially reported. The two measurements bracket the value reported in the Juda patent (USP 6,238,645).

A number of H_2 permeation tests were conducted on Pd-Cu membranes (9 and 12 μm-thick) and the results from this testing are presented below. Prior to testing the membrane in hydrogen at temperature, each membrane was tested with helium to insure a leak-tight seal. The first successful membrane to be tested was a 12.7 μm-thick foil with a composition slightly off of the ideal $Pd_{60}Cu_{40}$ (i.e., slightly higher Palladium weight fraction). The membrane was heated to 250°C, and the H_2 permeability at this temperature was determined to be $3.8 \bullet 10^{-5}$ $cm^3 \bullet cm/cm^2 \bullet s \bullet cm\ Hg^{-1/2}$ (For comparison, the permeability of a $Pd_{60}Cu_{40}$ foil at 250°C from the patent literature (USP 3,439474) is $5.5 \bullet 10^{-5}$ $cm^3 \bullet cm/cm^2 \bullet s \bullet cm\ Hg^{-1/2}$). This is good agreement given that the palladium composition of the foil sample is higher than 60 mass %.

Figure 28 shows molar flux versus driving force for this membrane at 250°C. The membrane was then heated up to 300°C. The flux declined to approximately one third of the value at 250°C. One possible reason for this could be carbon contamination from the o-ring. Upon removing the membrane from the cell, the o-ring appeared to have degraded. Another explanation could be that the membrane did not undergo a phase change to the higher permeability β -phase, and that it may have moved into the mixed α and β phase.

As shown in the phase diagram of Figure 29, if the composition of the Pd-Cu membrane is greater than boundary between the pure β and α/ β phase boundary (at an approximate palladium concentration (in weight percent) of 61%), then a two phase structure can exist and thereby reduce the efficiency of the membrane. For a constant composition, the membrane can transform from the single phase, β, to the two phase α + β, structure by merely heating up the membrane and thereby crossing the phase boundary.

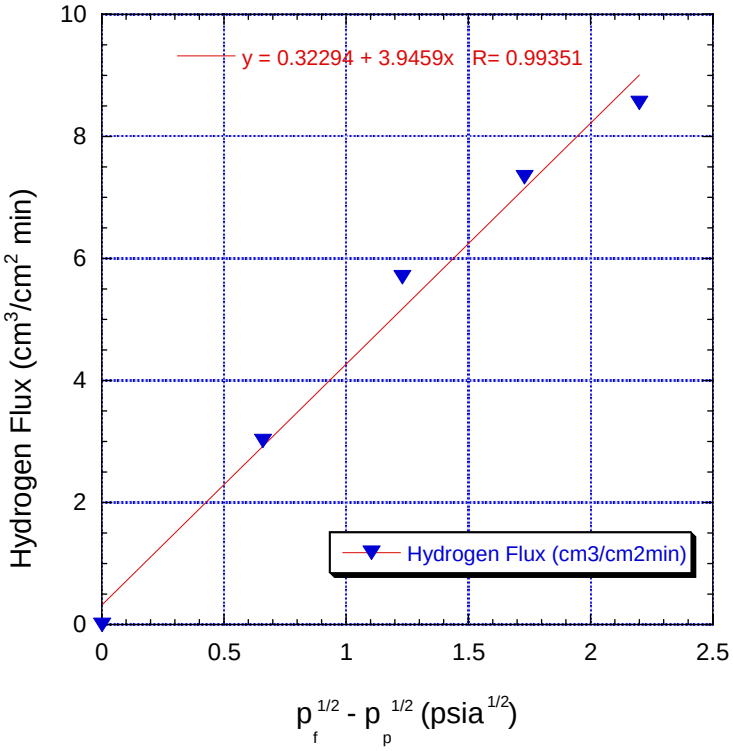

Figure 28. Pure hydrogen flux data at 250°C for 13 µm foil prepared by IBAD on silicon wafer support. Feed pressures range from 5 to 20 psig. Atmospheric pressure is 12 psia in Golden, CO.

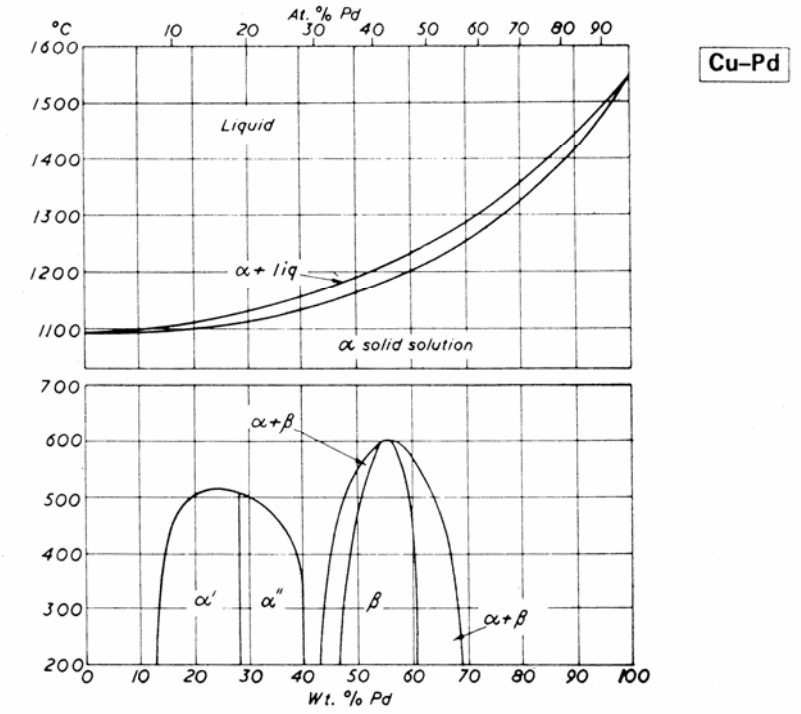

Figure 29. Pd-Cu phase diagram.

XRD analysis was performed on the treated 12.7 µm-thick membrane discussed above as well as on a piece of as-received foil; the treatment consisted of: 1) exposure to H_2 at 250°C for 24 hours, 2) 300°C for 72 hours, 3) 250°C for 24 hours, and finally, 4) air quench to room temperature. The XRD pattern is shown in Figure 30. Analysis indicates that the treated foil was in the β phase. Figure 31 shows the XRD pattern of an as received piece of foil. The pattern suggests that the material is in a mixed phase of both the α and β crystal structures.

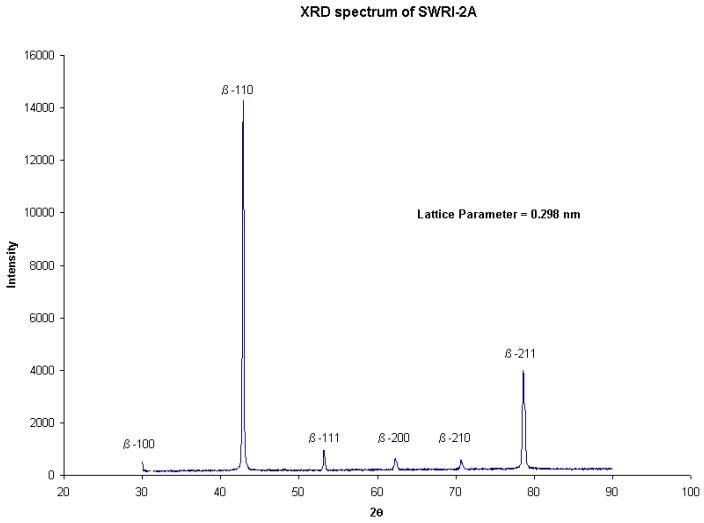

Figure 30. XRD pattern of heat treated PdCu foil

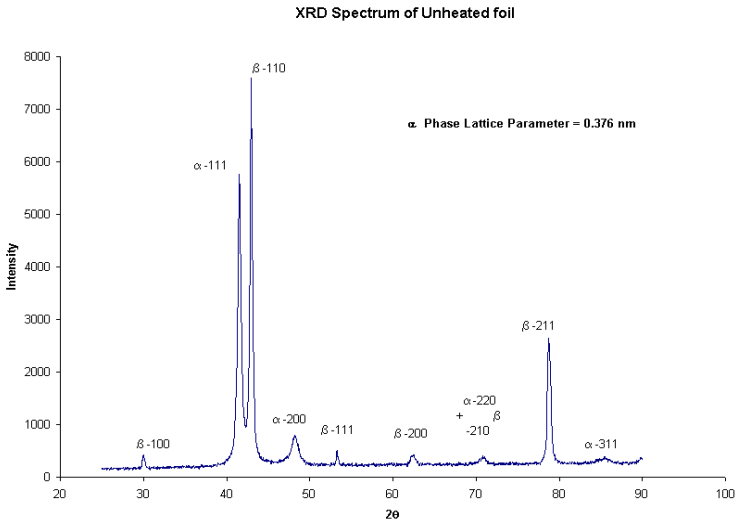

Figure 31. XRD pattern of as received PdCu foil

Another membrane (thickness ~ 12 µm) was sealed on an anodic support in the cell using a Kalrez® o-ring. The pure H_2 flux is shows graphically in Figure 32. The drop in flux between 250°C and 275°C was puzzling, however it is notable that the behavior appeared reversible. This could point to a phase change within the material at these temperatures.

An additional membrane, thickness ~ 9µm, displayed a pure hydrogen flux of 16.8 $cm^3(STP)/cm^2 \bullet min$; this is 2.2 times greater than that of the thicker membrane presented above at the same temperature and driving force.

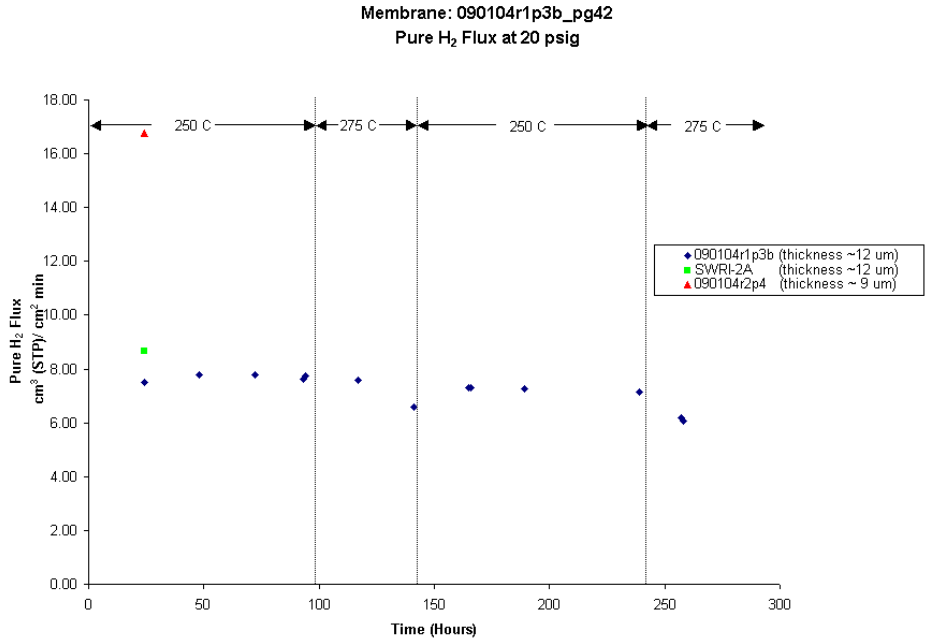

Figure 32. Pure hydrogen flux for a 20 psig feed pressure for various membranes

The H_2 permeability of the 9 μm-thick membrane above is $5.1 \cdot 10^{-5}$ $cm^3(STP) \cdot cm/cm^2 \cdot s \cdot cm\ Hg^{0.5}$. Correcting the permeability value to 350°C using the data in the McKinley patent (USP 3,439,474), we obtain a value of $7.4 \cdot 10^{-5}$ $cm^3(STP) \cdot cm/cm^2 \cdot s \cdot cm\ Hg^{0.5}$. This value compares well to the permeability reported by McKinley for a 62.5% Pd membrane of $7.9 \cdot 10^{-5}$ $cm^3(STP) \cdot cm/cm^2 \cdot s \cdot cm\ Hg^{0.5}$. Another comparison is that the hydrogen permeability of membrane (9 μm) is 56% of the value at the same temperature reported by McKinley for a Pd-Cu alloy membrane with the optimum 60% Pd composition. The discrepancies are attributed to differences in the Pd composition and the cold-rolled foils used by McKinley and Edlund.

Permeation testing was completed on 6 and 14 μm-thick Pd-Cu films. Membrane 080304r1p4 (thickness ~ 6 μm) was sealed in the cell using a Kalrez® o-ring. This membrane exhibited a small helium leak that was attributed to Knudsen diffusion (Pure hydrogen flux vs. driving force measurements showed a pressure dependence of ΔP^n where n was approximately 0.6), indicating that there is likely a pinhole in the membrane. All of the following hydrogen fluxes were corrected for the observed leak. The membrane was heated to 257°C under helium, and hydrogen flow to the membrane was initiated after remaining at 257°C for 12 hours. The hydrogen flow remained on, and the pure hydrogen flux at 20 psig was measured. The flux at these conditions slowly decreased from about 28 cm^3/cm^2 min to about 20 cm^3/cm^2 min over a period of 5 days. At this point, the flow to the membrane was switched from hydrogen to helium and left overnight with a feed pressure of 0 psig. After remaining under helium for approximately 15 hours, the membrane was tested again for pure hydrogen permeation at 20 psig. The pure hydrogen flux jumped to 36 $cm^3(STP)/cm^2$ min. The pure hydrogen flux was measured again at 36 cm^3/cm^2 min the following day after the membrane was exposed to helium again overnight. This flux corresponded to a pure hydrogen permeability of $7.4 \cdot 10^{-5}$ $cm^3\ cm\ cm^{-2}\ s^{-1}\ cm\ Hg^{-1/2}$ at 250°C. This value is within 20% of the pure hydrogen permeability at 250°C reported in the McKinley patent.

The furnace temperature was then ramped to 275°C. A temperature of 281°C was measured using a thermocouple probe placed inside the cell, on the feed side of the membrane. A continuous flow of pure hydrogen was used on the feed side of the membrane for several days and the pure hydrogen flux at 20 psig decreased steadily to about 14 cm^3/cm^2 min over this time period. The temperature was then ramped down again to 257°C and the pure hydrogen flux did not recover. It dipped slightly lower to 13 cm^3/cm^2 min. Repeating the procedure of leaving the membrane under helium at 0 psig overnight did result in a sharp increase in pure hydrogen flux back to 36 cm^3/cm^2 min, which subsequently began to decrease with time.

One hypothesis for the above behavior is that oxygen had been diffusing back through the permeate lines of the system and oxidizing the surface of the foil. To test this hypothesis, the feed side of the membrane was exposed to helium at 20 psig for 15 hours and then hydrogen flux was measured. The pinhole leak ensured that there was helium flow in the permeate lines when the feed side was pressurized to 20 psig. This would limit oxygen from diffusing back through these lines. Figure 33 below shows the behavior of pure hydrogen flux at 20 psig for these conditions.

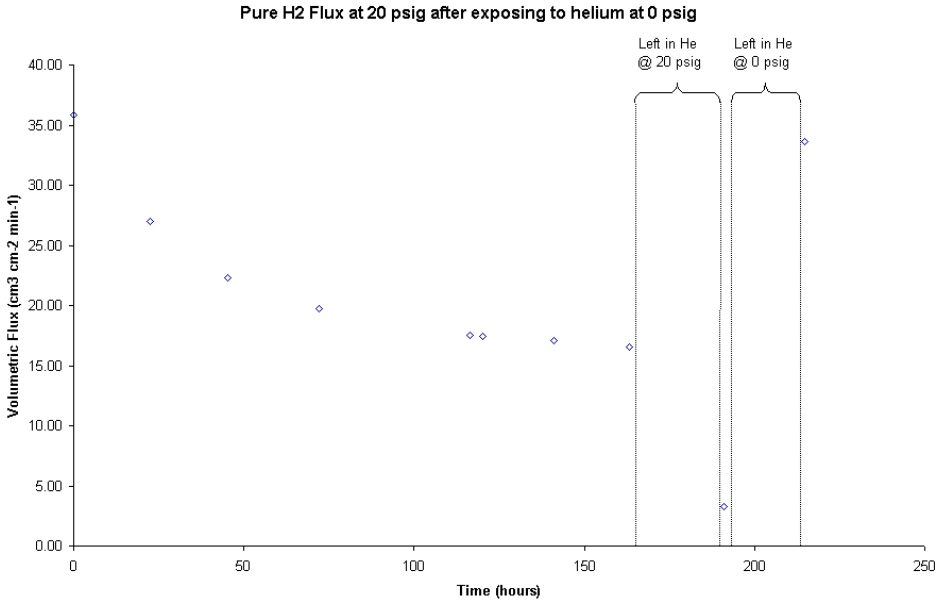

Figure 33. Pure hydrogen flux at 20 psig for membrane 083004r1p4 at 250°C.

The above figure clearly shows the peak in hydrogen flux after exposing the membrane to helium at 0 psig and the decreasing trend from 35.9 cm^3 cm^{-2} min^{-1} to around 16.5 cm^3 cm^{-2} min^{-1}, where the flux levels off. The enhanced hydrogen flux was not observed when the membrane was left under helium at 20 psig, instead, the flux decreased significantly. This supports the hypothesis that the enhanced hydrogen flux was a result of air oxidation of the foil. The flux recovered back to 33.7 cm^3 cm^{-2} min^{-1} when the membrane was exposed to helium at 0 psig for 15 hours, showing that the effect is reproducible.

Membrane 083104r1p2a (thickness ~14 μm) was placed into the Millipore fixture over a ceramic paper support and sealed using a graphite seal. The ceramic support ensured that there would be no intermetallic diffusion between the foil and the material that made up the Millipore fixture. Furthermore, the graphite seal provided the freedom to test at elevated temperatures.

The membrane was leak-free at room temperature and deemed acceptable for testing at high temperature. The system was brought to 250°C and left under hydrogen. Pure-gas flux measurements were made with a hydrogen feed pressure of 20 psig. The hydrogen permeate flow rate showed a gradual decreasing trend from 22.3 cm^3/min to 11.4 cm^3/min over a period of 210 hours. The temperature was then raised to 350°C to increase the rate at which any sort of phase change could be occurring. From this point on, the pure hydrogen flux began to increase. The system seemed to be approaching a steady state, with a pure hydrogen flux of 4.7 cm^3/cm^2 min and then the flux suddenly increased. Tests with helium gas revealed that a pinhole might have formed in the membrane, as there was a measurable helium flux of 0.7 cm^3/cm^2 min. Figure 34 shows the behavior of pure hydrogen flow-rate with respect to time at the two temperatures. The pure hydrogen flux measured before the leak corresponds to a hydrogen flux of $2.1 \cdot 10^{-5}$ $cm^3(STP) \cdot cm/cm^2 \cdot s \cdot cm\ Hg^{0.5}$. This value is considerably lower than the expected permeability of $Pd_{60}Cu_{40}$ materials at 400°C.

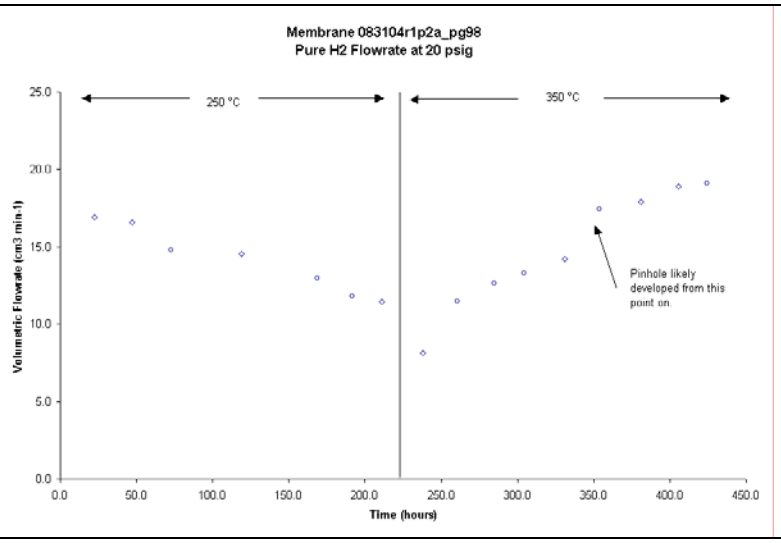

Figure 34. Influence of time on hydrogen permeation of membrane 083104r1p2a with a hydrogen feed pressure of 20 psig.

Figure 35. Image of Pd60Cu40 standard foil showing the apparent carbon contamination on the surface that appeared after testing.

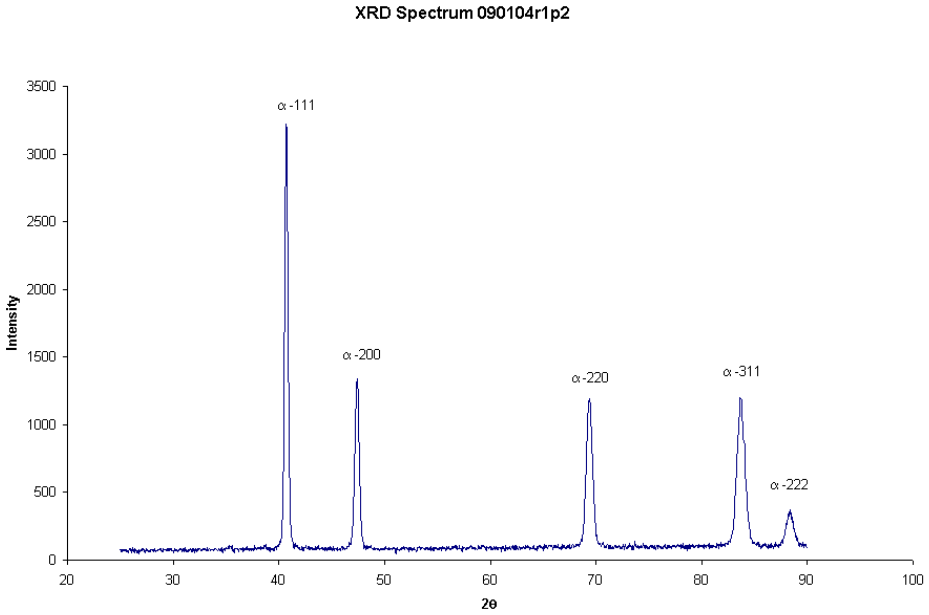

Figure 36. XRD pattern of membrane 090104r2p4 annealed at 450°C

A 25 µm thick palladium-copper foil known to be 60 wt.% Pd was obtained from IdaTech and was used as a standard for compositional analysis of subsequent membranes. A 25 mm disc of this material was tested for hydrogen permeation. The material was tested as received, with no prior activation. A steady-state measurement of pure hydrogen flux was performed and the hydrogen permeability at 400°C was calculated to be $7.2 \cdot 10^{-5}$ $cm^3(STP) \cdot cm/cm^2 \cdot s \cdot cm\ Hg^{0.5}$. This value is nearly 50% of the maximum permeability reported in the literature for $Pd_{60}Cu_{40}$ materials. Upon

examining the foil after testing, it appeared that the surface had significant carbon contamination that may have come from the graphite seal used in the membrane holder. See Figure 35 for an image of the surface of the membrane. This apparent carbon contamination could explain the why the permeability observed is lower than that reported in the literature.

An experiment was performed to determine the crystal structure of membrane 090104r1p2. The foil was annealed in nitrogen for 7 days at 450°C, and then rapidly quenched in an ice bath. The surface of the foil appeared slightly oxidized. Figure 36 shows the XRD pattern of this foil after annealing. This pattern suggests that the crystal structure is fcc and the foil is wholly in the α-phase. This is not consistent with the Pd-Cu phase diagram for a composition near 60 wt. % Pd. We expected to see peaks corresponding to both the α and β phases. EDS analysis of this sample showed a composition of 68 wt. % Pd, which is more consistent with the observed XRD pattern.

The composition of sample 083004r1p4 was determined, using EDS, to be 63 wt. % Pd and 37 wt. % Cu. Table 5 below shows the EDS analysis of this membrane as well as a 60 wt. % Pd and 40 wt. % Cu standard. The results at different spots were averaged and then normalized against the standard.

Table 5. EDS analysis of membrane 083004r1p4 and $Pd_{60}Cu_{40}$ standard from IdaTech

EDS Compositional Analysis

Sample	Spot	Pd wt. %	Cu wt. %
$Pd_{60}Cu_{40}$ Standard	1	60.71	39.29
	2	60.54	39.46
	3	61.97	38.03
	4	59.19	40.81
	5	59.32	40.68
	6	61.60	38.40
	7	61.14	38.86
	8	59.40	40.60
	9	59.37	40.63
083004r1p4	1	62.45	37.45
	2	63.14	36.86
	3	65.27	34.73
	4	63.33	36.67
	5	62.30	37.70
	6	63.22	36.78
	7	63.57	36.43

	Average Pd	Average Cu	Total
Standard	60.36	39.64	100.00
083004r1p4	63.33	36.66	99.99

	Standardized Pd	Standardized Cu	Total
Standard	60.00	40.00	100.00

The composition determined using EDS is reasonable as it corresponds well to the measured pure hydrogen flux. The steady state, pure hydrogen flux of membrane 083004r1p4 at 250°C was determined to be $3.3 \cdot 10^{-5}$ $cm^3(STP) \cdot cm/cm^2 \cdot s \cdot cm\ Hg^{0.5}$. The McKinley patent (USP 3,439,474) reports the pure hydrogen flux at 350°C for a membrane that is 62.5 wt.% Pd and 37.5 wt.% Cu as well as pure hydrogen fluxes for a 60 wt.% Pd foil at various temperatures. Using data from the patent and assuming that the activation energy for a 62.5 wt% Pd foil is the same as that of a 60 wt.% foil, the flux for the 62.5 wt.% foil at 250°C was estimated to be $5.2 \cdot 10^{-5}$ $cm^3(STP) \cdot cm/cm^2 \cdot s \cdot cm\ Hg^{0.5}$. This value compares reasonably well to the hydrogen permeability of membrane 083004, particularly considering that the composition is even further from the 60 wt. % Pd target so a lower permeability was expected.

Essentially all the vacuum deposited Pd-Cu thin film membranes had palladium compositions that were as much as 3% greater than the ideal 60 weight percent composition (this is a direct consequence of sputtering from a 60/40, Pd/Cu alloy target). As the concentration of Pd increased beyond the optimum 60% value, a less desirable two-phase structure formed at the higher temperatures (in this case, above 260 –280°C).

Membrane *SwRI-pg168* was prepared using magnetron sputtering and then tested for permeation with pure hydrogen. See Figure 37 for the hydrogen flux behavior with time at 400°C and 20 psi trans-membrane pressure. A helium leak of 1.1 cm^3 (STP)/ cm^2 min was observed at time, t ~ 51 hours indicating that a leak may have developed during testing. The data in Figure 37 have been corrected for this leak.

Table 6 shows the how the hydrogen flux of membrane *SwRI-pg168* compares to the targets established by the Office of Fossil Energy Hydrogen from Coal RD&D plan. The hydrogen flux at the target conditions is calculated based on the results at 20 psig. This foil exceeds the 2015 target.

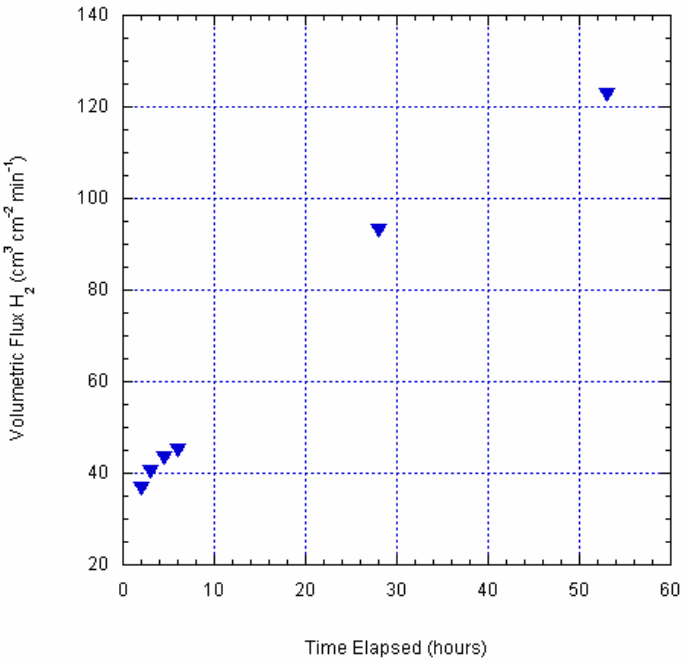

Figure 37. Influence of time on hydrogen permeation of membrane *SwRI-pg168* at 400°C with a hydrogen feed pressure of 20 psig.

Table 6. Calculated H_2 flux of membrane *SwRI-pg168* and Office of Fossil Energy performance targets

Performance Criteria	Membrane *SwRI-pg168*	2007 Target	2010 Target	2015 Target
Flux scf/h/ft2 @ 100 psi ΔP H_2 partial pressure & 50 psia permeate side pressure	564	100	200	300

The thickness of membrane *SwRI-pg168* was measured after testing in order to minimize handling of the film before hydrogen permeation could be studied and was measured with a micrometer to be 5 μm. The hydrogen permeability was then determined to be $2.0 \cdot 10^{-4}$ $cm^3(STP) \cdot cm/cm^2 \cdot s \cdot cm\ Hg^{0.5}$.

A separate sibling membrane, labeled *SwRI-pg176*, was also tested. This membrane was mounted as received using the same arrangement as *SwRI-pg168*. At 400°C and 20 psi, a helium leak of 7.4 cm^3(STP)/min is observed. The hydrogen flow rates were corrected for this leak. The hydrogen flow rate at 20 psi achieved a steady state of approximately 58 cm^3(STP)/min relatively quickly. An *in-situ* air oxidation was performed at 20 psig and 400°C for 1 hour, upon which the hydrogen flow rate doubled to a steady value of approximately 121 cm^3(STP)/min. A second air oxidation was then performed where air was supplied to the foil at 20 psig and 400°C for a period of 2 days. A jump in the hydrogen flow rate was observed followed by a gradual decrease to a higher steady state. Figure 38 shows the hydrogen flux behavior with time at 400°C and 20 psi trans-membrane pressure and the influence of air oxidation treatments. This foil exhibited dramatic enhancements in hydrogen flux as a result of air oxidation similar to the 25 μm foil.

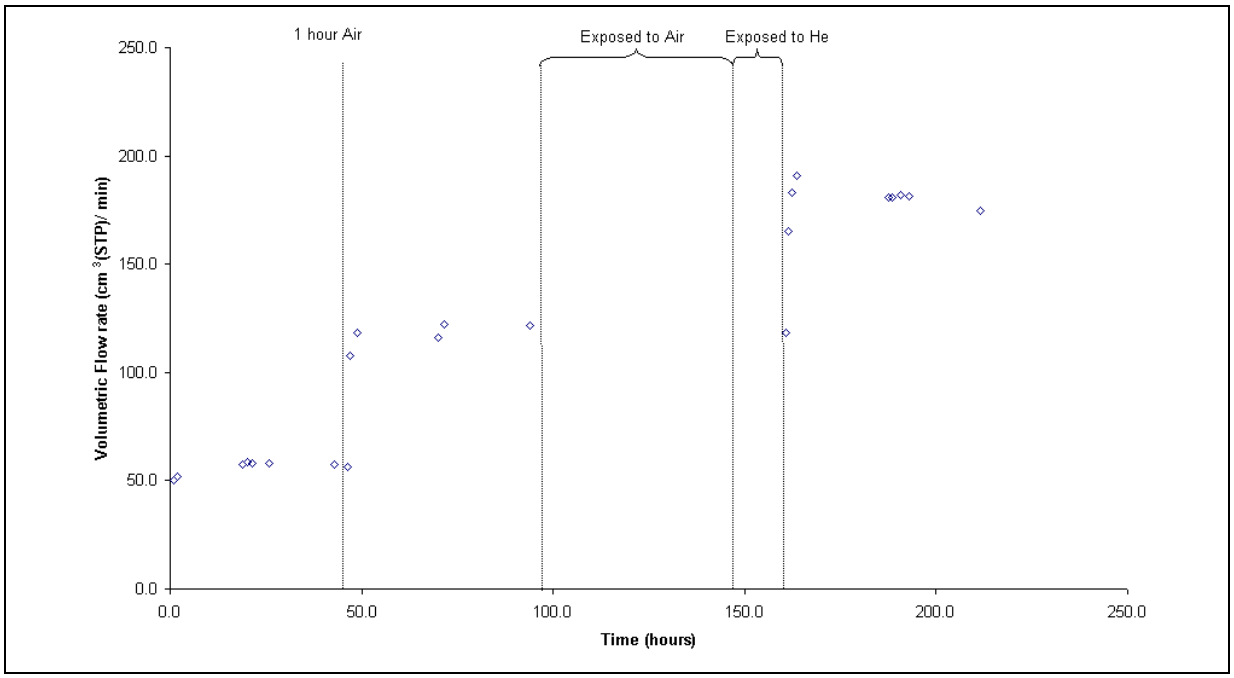

Figure 38. Influence of time and air oxidation on hydrogen permeation of membrane *SwRI-pg176* at 400°C with a hydrogen feed pressure of 20 psig.

A marked increase in membrane performance primarily due to proper alloy composition and pre-treatment procedures was observed. As an example, the hydrogen flux at 400°C and 20 psi trans-membrane pressure, for a 5 µm-thick membrane, was 120 cm^3 (STP)/cm^2 min. The productivity of this membrane exceeds the 2015 DOE Fossil Energy targets. Hydrogen permeability was calculated to be $2.0 \cdot 10^{-4}$ cm^3(STP)•cm/cm^2•s•cm $Hg^{0.5}$. Permeation tests were then repeated on a sibling membrane sample and the measured hydrogen flow rate at 400°C and 20 psi was 58 cm^3 (STP)/min. Although lower than the flow rate of the first sample, the hydrogen flow rate increased to 175 cm^3 (STP)/min after two oxidation treatments.

Permeation experiments continued with *SwRI-pg176*. Figure 39 shows the hydrogen flux behavior with time at 400°C and 20 psi trans-membrane pressure and the influence of air oxidation treatments. The hydrogen flux at 20 psi achieved a steady state of approximately 28 cm^3(STP)/ cm^2 min relatively quickly. An *in-situ* air oxidation was performed at 20 psig and 400°C for 1 hour, upon which the hydrogen flux doubled to a steady value of approximately 59 cm^3(STP)/ cm^2 min. A second air oxidation was then performed where air was supplied to the foil at 20 psig and 400°C for a period of 2 days. A jump in the hydrogen flux was observed followed by a gradual decrease to an even higher steady state of 78 cm^3(STP)/ cm^2 min. A subsequent oxidation resulted in a spike in the hydrogen flux, but eventually declined back to the previous steady state. The pure hydrogen permeability (measured at steady state after ~330 hours) was determined to be $1.3 \cdot 10^{-4}$ cm^3(STP)•cm/cm^2•s•cm$Hg^{0.5}$. This permeability was calculated from the steady-state H_2 flux and a thickness of 5 µm (as determined with micrometer gauge). It is worth noting that this permeability corresponds to a flux of 187 ft^3(STP)/ft^2•h for a hydrogen partial pressure difference of 50 psi, which meets the DOE Fossil Energy flux target for 2007.

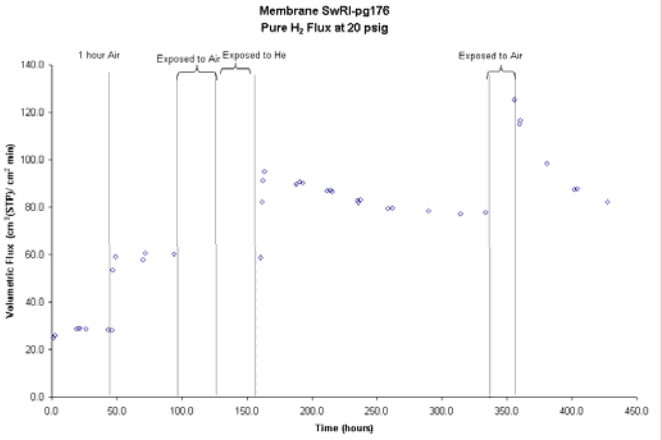

Figure 39. Influence of time and air oxidation on hydrogen permeation of membrane *SwRI-pg176* at 400°C with a hydrogen feed pressure of 20 psig.

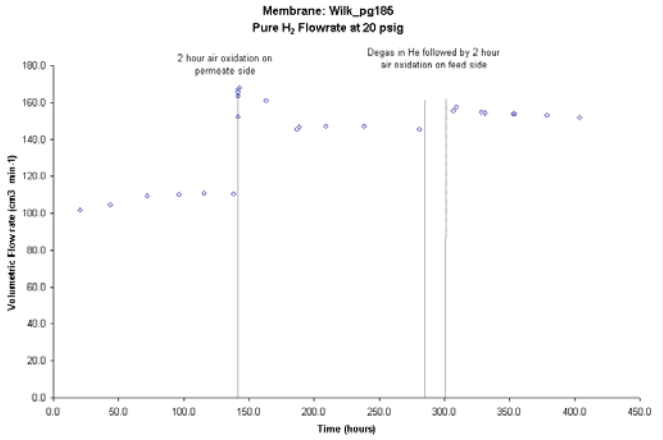

Figure 40. Influence of time and air oxidation on hydrogen permeation of membrane *wilk_pg185* at 400°C with a hydrogen feed pressure of 20 psig.

It should also be noted that this membrane displayed a helium leak that increased over time from about 3.7 to 9 cm^3(STP)/ cm^2 min. The hydrogen flux was corrected for this leak.

An investigation of the air oxidation effect continued with the 25 μm control foil. See Figure 40 for a graph of hydrogen flow rate vs. time for *wilk_pg185*. This foil was heated in air ex-situ at 400°C for 2 hours. This presumably cleans the surface of contaminants. The membrane was then mounted and heated to 400°C in helium followed immediately by an *in-situ* air oxidation of the feed side. At this point, the membrane exhibited a slightly increasing hydrogen flow rate of about 110 cm^3(STP)/min. Next, the permeate side of the membrane was exposed to air at the same conditions. A hydrogen flux increase of ~50% was measured. This supports the hypothesis that the hydrogen flux increase is a result of surface effects. Another possibility is that carbon contamination inside the membrane (possibly from the fabrication procedure) is not completely removed after only the *in-situ* feed side oxidation. As a control, the feed side of the membrane was exposed to air a second time to investigate its effect on hydrogen permeability. The flux marginally increased, indicating that the surface morphology did not change dramatically or that carbon contamination in the membrane was almost completely removed after the second *in-situ* oxidation.

Membranes, up to 10 μm-thick, were also tested and results for a representative film, *SwRI-pg203*, are presented below. Initially, this membrane was heated to 250°C in helium and subsequently tested for hydrogen permeation. After 15 hours of testing, there was essentially no hydrogen permeation through the membrane at 250°C. With a 20 psi trans-membrane pressure, a hydrogen flux of only 0.3 cm^3(STP)/cm^2 min was measured. The temperature was then ramped to 400°C, and the hydrogen flux began to increase yet remained lower than expected. Figure 41 shows the data set for this membrane after the temperature was increased to 400°C. The feed side of this membrane was exposed to air at 10 psig for 2 hours at 400°C *in-situ*. The time of the air exposure is marked on Figure 41 by the dotted vertical line at approximately 85 hours. As seen in the figure, the hydrogen flux rapidly increased to a steady hydrogen flux of 32 cm^3(STP)/cm^2 min after the air exposure.

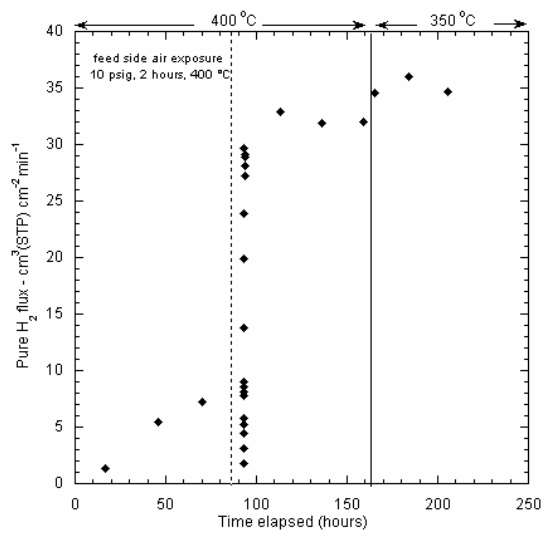

Figure 41. Influence of time and air oxidation on hydrogen permeation of membrane *SwRI-pg203* at 400°C with a hydrogen feed pressure of 20 psig.

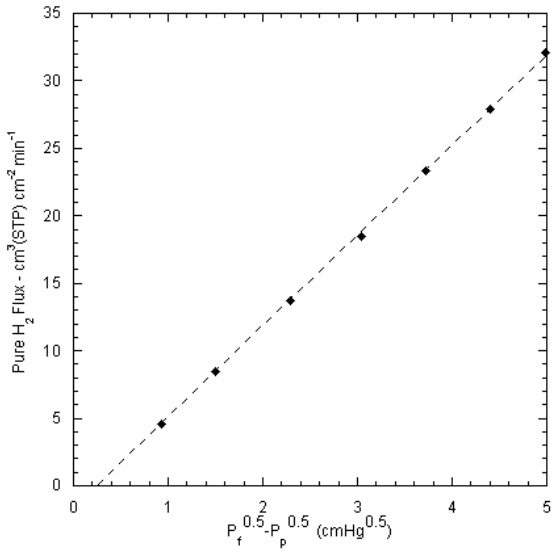

Figure 42. Pure hydrogen flux at 400°C vs. driving force for membrane *SwRI-pg203*.

Figure 42 shows the pure hydrogen flux vs. driving force once this steady value was achieved. From the data in this figure, the n-value was determined to be 0.59, indicating that the measured transport through the system may not be completely governed by solution diffusion in the bulk of the metal foil. However, the hydrogen/helium ideal separation factor at 20 psig and 400°C was determined to be greater than 100,000. This reveals that the membrane was mostly defect free. Hence, Knudsen diffusion through the foil should not play a significant role in the transport mechanism and therefore is unlikely the reason for the deviation in the n-value. A possible reason for the slightly larger n value for this membrane could be contamination on the feed side such as carbon.

Based on SEM images of the cross-section of the foil (one of which is shown in Figure 43), an average membrane thickness was determined to be 9.7 μm. This is significant, in that it demonstrates that even a membrane approximately 10 μm thick can exceed the DOE's hydrogen flux target. Additionally, this value was used to calculate a pure hydrogen permeability of $1.1 \cdot 10^{-4}$ $cm^3(STP) \cdot cm/cm^2 \cdot s \cdot cm\ Hg^{0.5}$.

Crystalline structure analysis was performed using XRD after hydrogen permeation. The membrane was cooled relatively quickly from the last testing condition of 350°C and it was presumed that the crystal structure reflects that temperature condition. The diffraction pattern is shown in Figure 44. It is interesting to note that there are prominent α and β -phase peaks observed. Based on the Pd-Cu phase diagram, the α-phase was not expected at 350°C given the composition of 60.25 wt% Pd mentioned above. Additionally, the hydrogen permeability of this membrane was relatively high, suggesting that the foil would be mostly or all in the higher permeability β -phase. EDS analysis was performed here to confirm the alloy composition. The composition measured here was determined to be 62.96 wt. % Pd. This is more consistent with the crystal structure determined by XRD, but less consistent with the high permeability measured that corresponds to an alloy composition at or very near to 60 wt. % Pd.

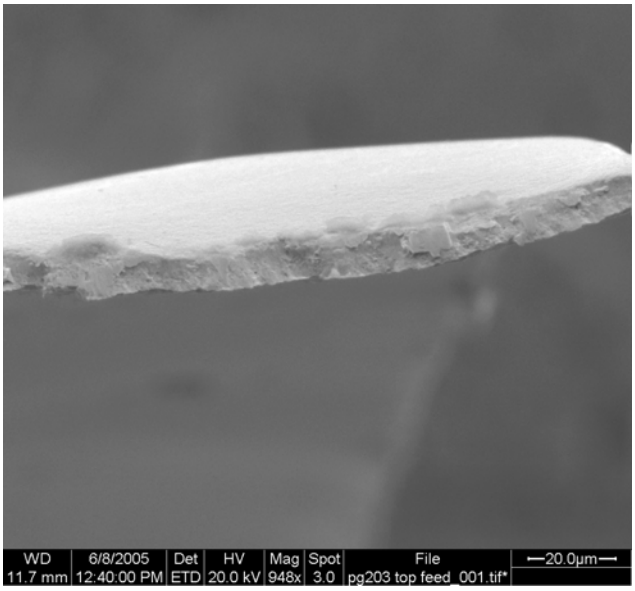

Figure 43. Cross-sectional image of membrane *SwRI-pg203*.

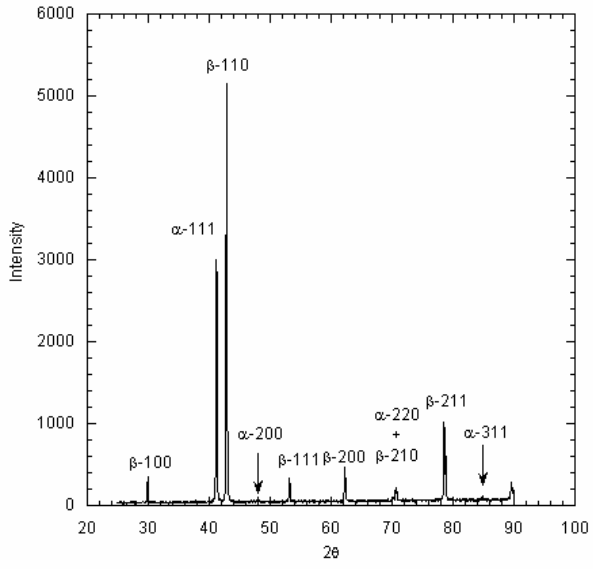

Figure 44. Diffraction pattern of membrane *SwRI-pg203* after permeation testing at 350°C.

Table 7 summarizes the most of the membrane tests that were conducted at CSM over 6 months from mid 2005 to early 2006. While difficulties were encountered with sealing the thinner membranes, tests on multiple samples from the same batch appear to exhibit reasonably consistent performance.

Table 7. Summary of Membranes Tested at CSM

Sample Number	Test Date	SwRI Pd %	Max Flux @ 400C & 20psi [cm^3/cm^2·min]	CSM Thickness [microns]	Permeance @ 400C [cm^3(STP)/cm^2·s·$cmHg^{0.5}$]	Permeability @ 400C [cm^3(STP)·cm/cm^2·s·$cmHg^{0.5}$]
41805SI1	7/12/2005	59.47	42.7	6.00	0.105	6.30E-05
42005SI1	10/11/2005	60.35	43.2	6.80	0.111	7.55E-05
092805#2	1/13/2006	58.41	18.2	2.60	0.060	1.57E-05
092805#2	1/21/2006	58.41	3.2	2.60	0.011	2.86E-06
092805#2	3/8/2006	58.41	N/A	9.20	N/A	N/A
100405#2	1/12/2006	59.57	N/A	3.00	N/A	N/A
100705#1	2/21/2006	60.73	10.2	4.00	0.034	1.35E-05
100705#2	11/10/2005	59.48	66.9	9.00	0.142	1.28E-04
100705#2	2/6/2006	59.48	5.41	9.00	0.018	1.62E-05
100705#2	3/11/2006	59.48	10.6	9.00	0.035	3.16E-05
101005#1	10/23/2005	59.82	N/A	3.30	N/A	N/A
101005#1	10/24/2005	59.82	36.7	5.29	0.114	6.03E-05
101005#1	2/6/2006	59.82	N/A	3.30	N/A	N/A
101205#2	10/22/2005	59.85	N/A	9.00	N/A	N/A
101205#2	2/21/2006	59.85	N/A	2.50	N/A	N/A

Hydrogen permeation experiments and characterization of 5 and 10 μm-thick, Pd-Cu films with compositions near the 60/40 (Pd/Cu phase boundary) in combination with air oxidation treatments to improve performance found pure hydrogen permeability for an as-received, 5 μm film at 400°C was determined to be 1.3×10^{-4} cm^3(STP)·cm/cm^2·s·$cmHg^{0.5}$ at steady state. Even a membrane ~ 10μm-thick, exhibited a steady state hydrogen flux of 32 cm^3(STP)/cm^2min after air exposure, which, when normalized for DOE's Office of Fossil Energy's specified hydrogen flux with a ΔP of 100 psi and a permeate pressure of 50 psia, results in a flux of 155 scfh/ft^2 (this flux exceeds the 2007 target by 55% and is a significant fraction (i.e. 77%) of the 2010 target).

Hydrogen permeation experiments were performed on a 6 micron-thick film (sample 41805SI1) in 50°C increments from 300-600°C. As expected, the pure hydrogen permeability increased up to 400 °C while the membrane was in the β-phase and dropped once the temperature increased to over 450°C. According to the Pd-Cu phase diagram shown in Figure 29, this temperature corresponds to theα and β mixed phase. Figure 45, shown below, presents the pure H_2 permeability versus temperature data.

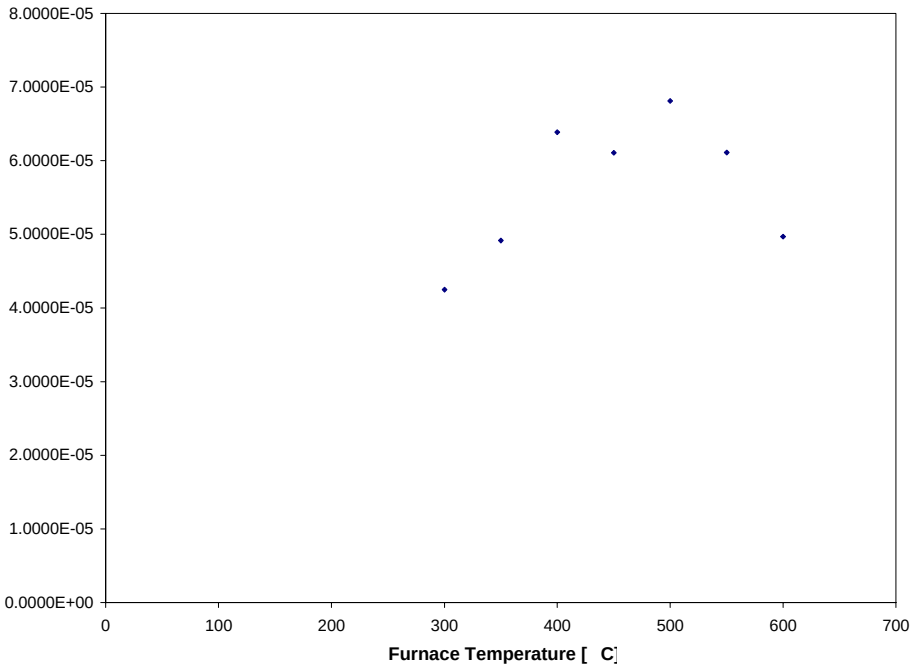

Figure 45. Pure Hydrogen Permeability versus Furnace Temperature

The same trend was observed for a 25 micron-thick foil (from Wilkinson) where the pure hydrogen permeability increased with temperature while the membrane was in the β-phase (as confirmed by XRD). Between 400 and 450°C, the membrane shifted to the α and β mixed phases, and the permeability dropped.

During testing, it appeared as though a leak formed in the 6 micron-thick, sputtered membrane as the temperature was raised above 500°C. This was verified through SEM imaging of the membrane surface which showed the formation of several pinholes (Figure 45). As was seen with the 6 micron-thick membrane, the Wilkinson foil also developed pinholes after being exposed to a temperature of 600°C. The Wilkinson foil's H_2/He selectivity remained high even though pinholes were beginning to form.

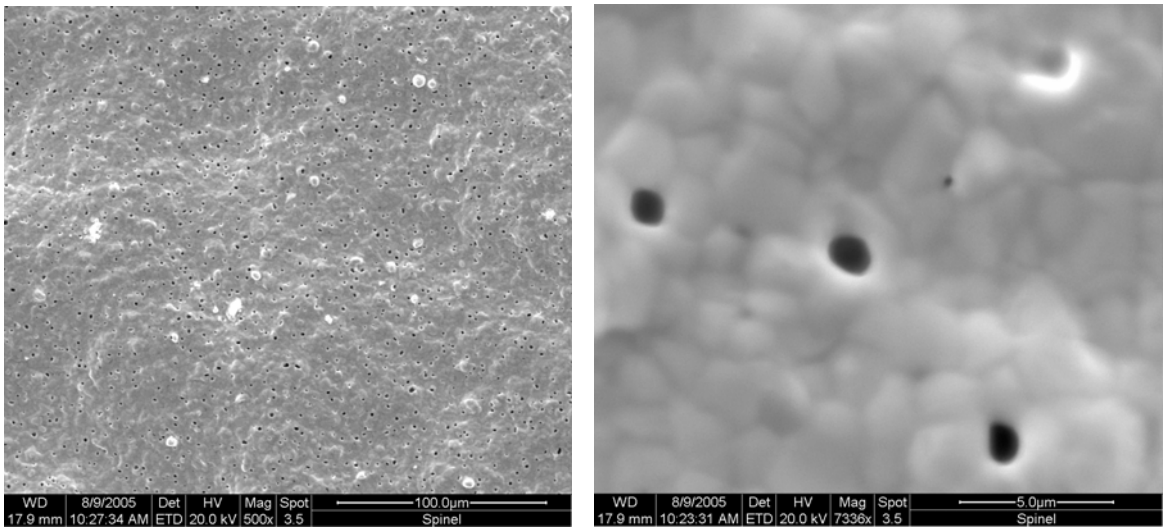

a) b)

Figure 46. SEM Image of 6 micron film from a) center of film at 500X and b) close up at 7338X.

Some difficulties were encountered with thinner membranes rupturing after heating to 300-450°C. A number of membranes were assembled and found to seal acceptably at room temperature but subsequently developed significant leaks upon heating. A preconditioning procedure was developed in which the membranes were first annealed in forming gas at 400°C for about 24 hours. The membranes were typically pressed between two flat alumina blocks to minimize curling during the annealing process. Two membranes, 100705#2 and 092805#2, showed negligible leak rates and were tested.

After pre-annealing in forming gas, one particular sample (100705#2) was tested at a driving force of 20 psi and no helium was found to leak through the membrane at room temperature. Once the furnace reached 400°C, the helium leak rate was measured and again found to be zero. The feed was switched to hydrogen and measurements were taken periodically until the flow reached steady state. Figure 46 shows the pure hydrogen flux for a 20 psi driving force at 400°C over a period of approximately 300 hours. This assumes 3.5 cm diameter of membrane exposed to the hydrogen flow (9.5 cm^2 area).

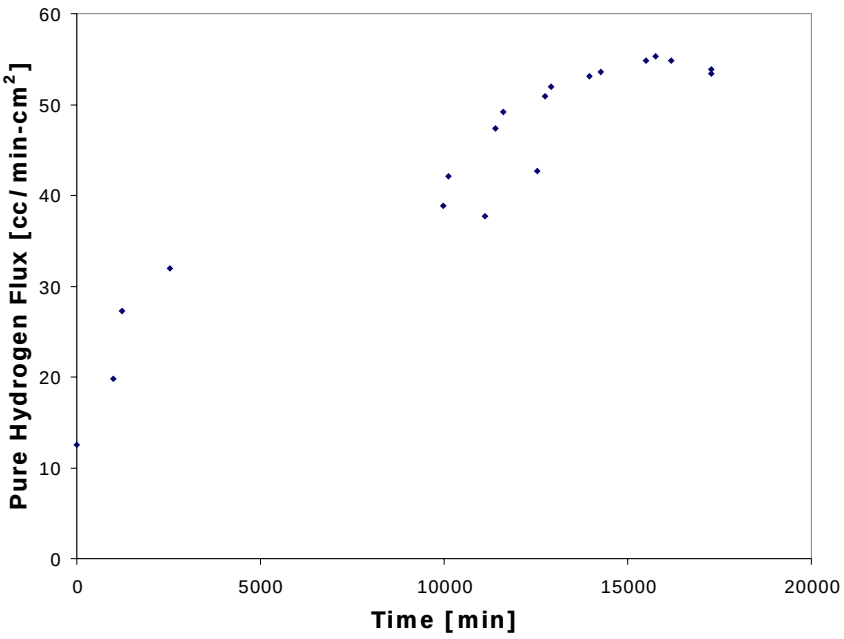

Figure 47. Membrane 100705#2 approaching steady state at 400°C and 20 psi

The final points on the plot correspond to a hydrogen flow rate of around 700 cc/min from which value of 1.11E-4 $cm^3 \cdot cm/cm^2 \cdot s \cdot cmHg^{0.5}$ was calculated at 400°C. At steady state, the membrane permeability was calculated at 300, 350, and 450°C using the measured thickness of 6 μm. These were then plotted with the Wilkinson and McKinley permeabilities for comparison. This plot suggests that this membrane was close to the ideal target composition of 60% Pd. The Wilkinson foils have been analyzed by EDAX using a traceable standard and the palladium weight percent is about 59.7%. Figure 47 shows the comparison of the Wilkinson membrane, McKinley patent data, and membrane 100705#2. The selectivity of this membrane was perfect throughout this extended permeation test, meaning that the flux of He was undetectable at 20 psig.

Using the measured H_2 permeability at 400°C, a flux could be calculated to compare with the DOE Fossil Energy targets. For a feed stream at 150 psia, the permeate stream at 50 psia, the pure H_2 flux for this membrane would be 255 SCFH/ft^2, exceeding the 2010 target of 200 SCFH/ft^2. If the thickness could be reduced from 6 μm to 5 μm with out negatively affecting the permeability, the 2015 target could be reached.

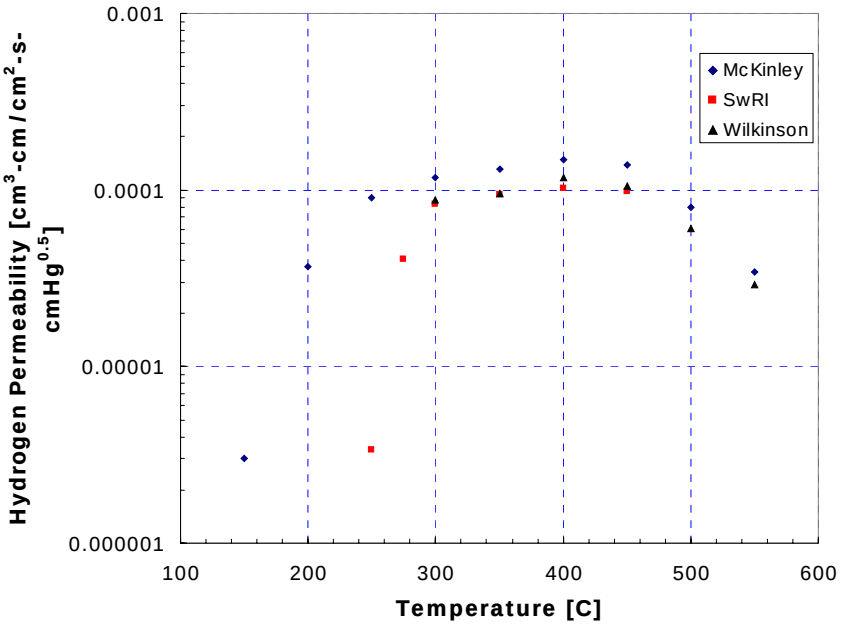

Figure 48. Permeability versus temperature plot for membrane 100705#2, Wilkinson foil, and McKinley patent data

A 3.5 micron Pd-Cu foil (092805#2) was annealed in forming gas at 400°C for 12 hours, placed in the test cell, and tested for helium leaks. There was no measurable helium leak out the sides of the membrane cell and the pressure did not change over a couple minutes when the feed and retentate streams were closed. The furnace was then set to 400°C where there was still no He leak from the cell. Figure 48 shows the membrane's approach to steady state. Overnight, the hydrogen feed flow rate is typically reduced to conserve H_2.and minimize any chance of emptying the gas bottle which is the source of the changes in flux. While the membrane seems to be slowly reaching a steady state and the total flux is significantly higher than 100705#2, it did not appear that the membrane would reach the expected flux based on the 3.5 micron thickness. A lower concentration of palladium in this membrane, 58.49%, is the likely cause of the reduced flux.

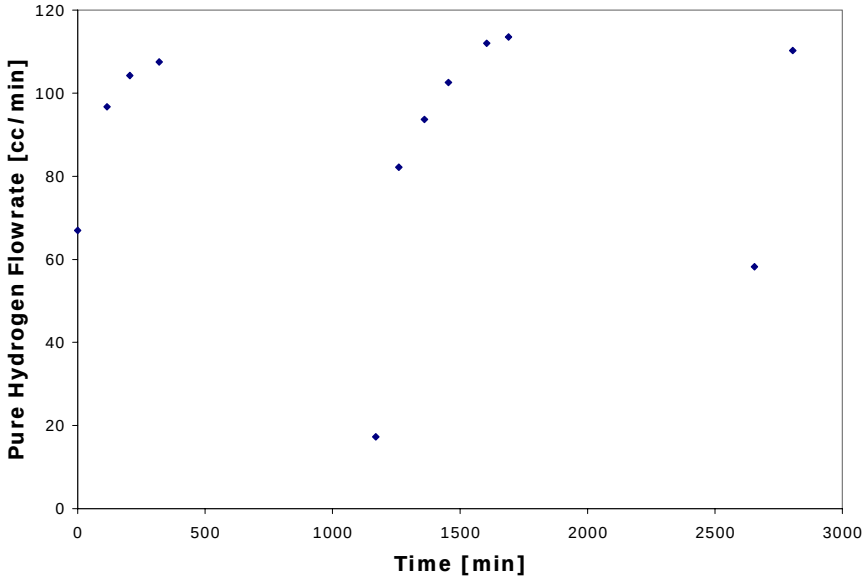

Figure 49. Membrane 092805#2 approaching steady state at 400°C and 20 psi.

CSM continued hydrogen permeation testing of SwRI fabricated membranes while investigating methods to anneal samples and bond samples together to seal pinholes. Membrane 031406#2 was a ternary alloy with rhodium. The thickness was found to be 7.47 μm. After testing at 400°C, the sample was heated to 525°C for 10 hours to anneal the membranes. The hydrogen flux through a 1-inch diameter sample did not change after annealing. The final value was 1.48 $cm^3(STP)/cm^2 \cdot min$ at 400°C and 20 psi. For a 2-inch sample, the hydrogen flux increased from 4.16 to 9.06 $cm^3(STP)/cm^2 \cdot min$ at 400°C and 20 psi. This is an increase of a factor of 2 after annealing. The helium flux also increased by a similar factor (0.408 to 0.880 $cm^3(STP)/cm^2 \cdot min$ at 400°C and 20 psi). The corresponding hydrogen permeability for the 2 inch sample was $3.5 \bullet 10^{-6}$ $cm^3(STP)cm/cm^2 \cdot s \cdot cmHg^{0.5}$.

Figure 49a and 49b show a significant change in the surface structure of the before and after samples based on SEM examination. The sample was not annealed before testing, but an air purge was run during testing. EDAX of the surface found a slight increase in the palladium composition after testing. The compositions were 43.62%Cu, 50.56%Pd, and 5.83%Rh and 41.68%Cu, 52.06%Pd, and 6.26%Rh before and after testing, respectively.

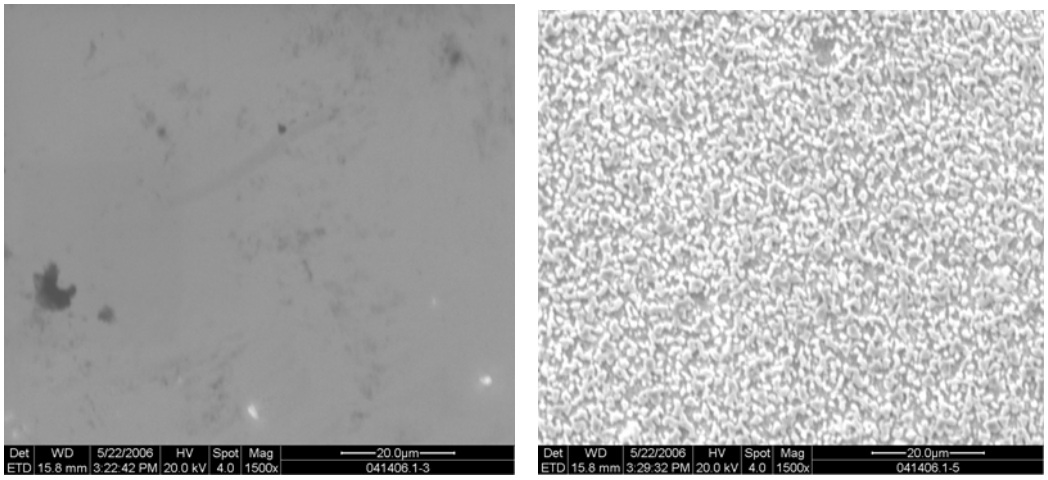

a) b)

Figure 50. Before (a) and after (b) testing SEM surface images of membrane 031406#2

Sample 030206#1, a Pd-Cu-Ru membrane, was tested for 11 days. The pure hydrogen flux reached 15.1 cm^3(STP)/cm^2·min at 400°C and 20 psi, but over the course of testing a substantial nitrogen leak developed. Therefore, the hydrogen flux and corresponding permeability are somewhat suspect. Roughening of the surface after testing was observed similar to the Pd-Cu-Rh sample. However, the surface of the Ru-doped membrane showed a significant change in composition. Before testing, the membrane was 44.61%Cu, 52.32%Pd, and 3.07%Ru. The palladium composition rose significantly after the testing and the final feed surface composition was 7.11%Cu, 90.57%Pd, and 2.32%Ru.

SEM, XRD, and EDAX analysis was done on selected samples from batch 051206#1 (Pd-Cu alloy). The XRD results showed that the as-received membranes were in the pure alpha phase while the annealed samples were purely beta (Figure 50). SEM images indicated that the membrane was unchanged during the annealing process.

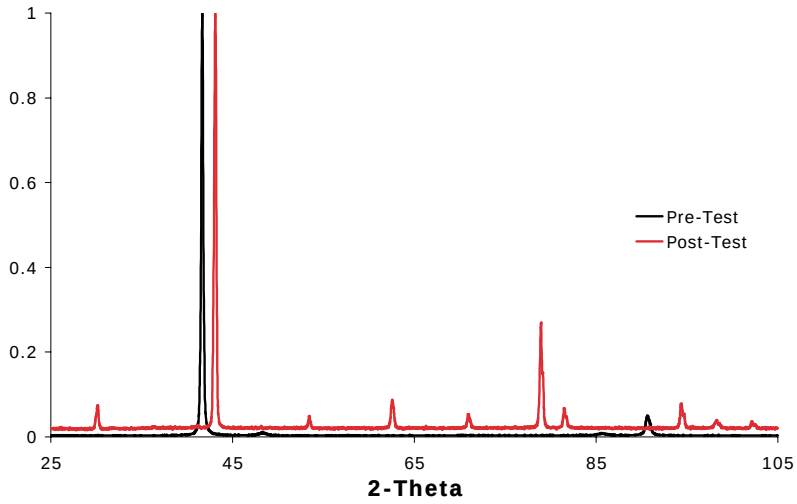

Figure 51. XRD spectrum of 051206#1 before and after testing

In an effort to fully understand the effect of annealing on these Pd-Cu membranes, a 2-inch un-annealed sample of 051206#1 and a 1-inch sample of the Wilkinson 25 micron thick, $Pd_{60}Cu_{40}$ standard foil were annealed at 400°C for 8 hours. The atmosphere was set to forming gas, but as has been seen before the membrane samples were oxidized. The two samples were then loaded into the test cells with no helium leak at room temperature. The furnace was ramped at 3°C per minute to 400°C where the helium flux remained zero throughout heating. The membranes remained under helium at 400°C for 24 hours with no permeation of helium. The membranes were then exposed to hydrogen. Upon hydrogen exposure, the Wilkinson standard started with a low flux (1.61 $cm^3(STP)/cm^2 \cdot min$) at 400°C and 20 psid while the SwRI sample tore. The Wilkinson foil reached a flux of 2.98 $cm^3(STP)/cm^2 \cdot min$ at 400°C and 20 psig and was then purged with air. At the same conditions, the flux reached 13 $cm^3(STP)/cm^2 \cdot min$.

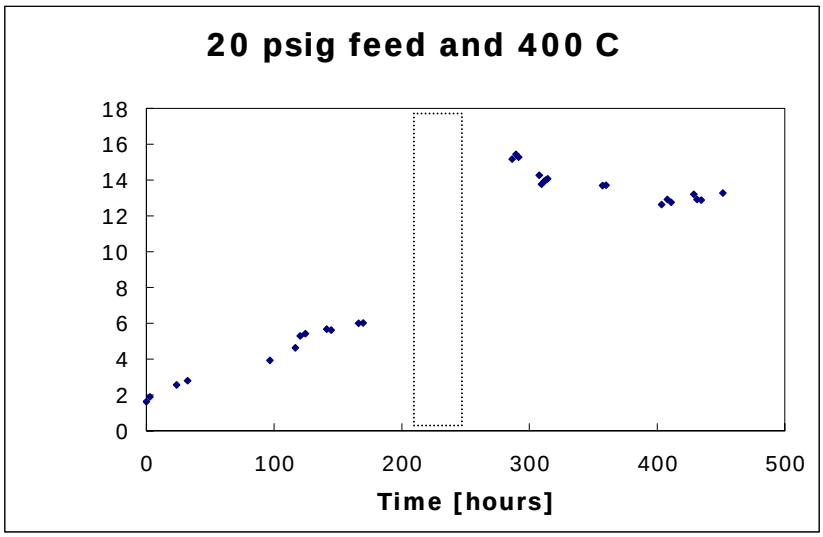

Figure 52. Wilkinson foil flux over time at 400°C and 20 psid

The air purge, denoted by the box in Figure 52, significantly raised the flux of the Wilkinson membrane. This has also been observed previously with the SwRI membranes. The final flux corresponds to a permeability of 1.1×10^{-4} $cm^3(STP) \cdot cm/cm^2 \cdot s \cdot cmHg^{0.5}$ at 400°C. This is in good agreement with the data for Wilkinson foil samples from previous measurements at CSM.

One of the samples from batch 051206#1 that was annealed at SwRI was sprayed with palladium acetate, oxidized, and then reduced. This process added palladium to the membrane which raised the composition from 57%Pd to 60%Pd.

A list of samples that CSM attempted to test in mid 2006 are listed in Table 8. Selected samples were also characterized using at SwRI and CSM XRD, SEM, and EDS.

Table 8. Samples tested at CSM, N/A indicates the sample tore or developed a leak during testing.

Sample Number	Date	Maker Pd %	EDAX Pd %	Max Flux @ 400C & 20psi [cm^3/cm^2·min]	CSM Thickness [microns]	Source	Maker Thickness	Permeance @ 400C [cm^3(STP)/cm^2·s·$cmHg^{0.5}$]	Permeability @ 400C [cm^3(STP)·cm/cm^2·s·$cmHg^{0.5}$]
051206#1	7/25/2002	---	57.00	17.9	8.80	SEM	---	5.98E-02	5.26E-05
051206#1	7/25/2002	---	57.00	30	8.80	SEM	---	1.00E-01	8.83E-05
072806#1	8/6/2002	62.00	---	N/A	---	SwRI	4.40	N/A	N/A
072806#1	8/27/2002	62.00	---	22.21	4.40	SwRI	4.40	5.14E-02	2.26E-05
073106#1	8/6/2002	62.00	---	N/A	---	SwRI	4.40	N/A	N/A
073106#1	8/7/2002	62.00	---	N/A	---	SwRI	4.40	N/A	N/A
073106#1	8/7/2002	62.00	---	N/A	---	SwRI	4.40	N/A	N/A
073106#1	9/10/2002	62.00	---	19.3	4.40	SwRI	4.40	6.46E-02	2.84E-05

Two membranes from batch 051206#1 were tested. One of the membranes was annealed in argon gas at SwRI and the other was tested as received. The annealed membrane leaked helium at room temperature, but once it reached 400°C the helium leak disappeared. The as received membrane did not leak helium at room temperature or 400°C. The steady state permeabilities at 400°C were $2.54x10^{-5}$ and $1.17x10^{-5}$ cm^3(STP)cm/cm^2·s·$cmHg^{0.5}$ for the as received and annealed samples, respectively. An air purge was then done for 90 minutes on each membrane. The final steady state permeabilities at 400°C and were $8.83x10^{-5}$ cm^3(STP)cm/cm^2·s·$cmHg^{0.5}$ for the as received membrane and $5.26x10^{-5}$ cm^3(STP)cm/cm^2·s·$cmHg^{0.5}$ for the annealed sample. The pure H_2 permeability of 8.83×10^{-5} cm^3(STP)cm/cm^2·s·$cmHg^{0.5}$ was very comparable to that measured for the highest flux membrane that was tested by an independent third party lab. The IdaTech permeability for the $Pd_{60}Cu_{40}$ alloy is about 1.2×10^{-5} cm^3(STP)cm/cm^2·s·$cmHg^{0.5}$ at 400°C.

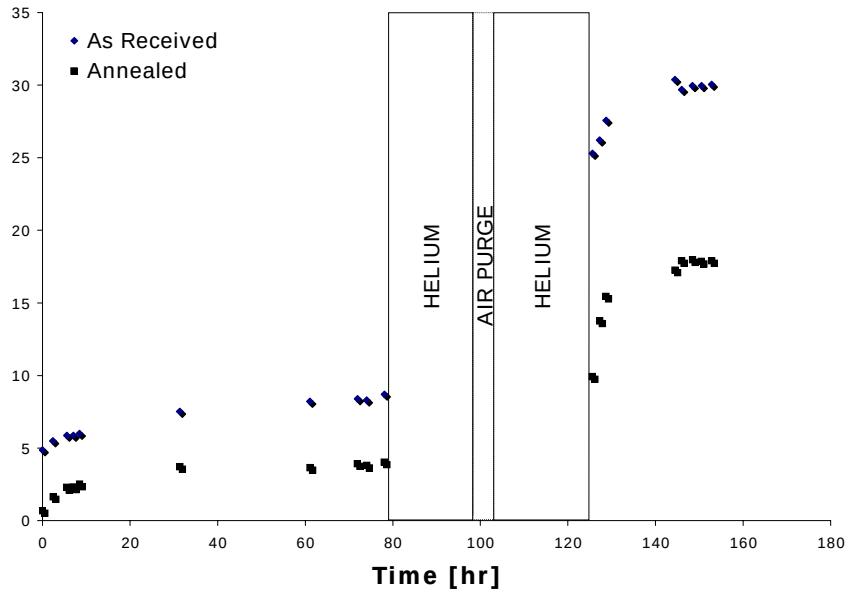

Figure 53. Pure hydrogen flux versus time for annealed and as received samples 051206#1

Although the permeability of the as-received material was not double the annealed sample, the fact that the permeability was higher for the as received sample is consistent with previous samples from this batch. Figure 53 shows the flux versus time for both membranes. The air purge significantly increased the flux for both samples. For this reason, the remaining membranes were purged once the furnace reached 400°C. This decreased the time it took for the membrane to reach steady state. The permeability values were higher than previously reported for the same samples. The previous permeabilities were $6x10^{-5}$ and $3x10^{-5}$ $cm^3(STP)cm/cm^2 \cdot s \cdot cmHg^{0.5}$ for the as received and annealed samples respectively. The higher permeabilities were attributed to composition differences in the samples. A slightly higher palladium composition resulted in a significant difference in the permeability.

Two samples from batch 032406#1 were annealed for 8 hours at 400°C in forming gas to reduce the stress in the membranes. These samples were loaded and had helium leaks of 0.64 and 19.0 cm^3/min at room temperature. They were heated to 400°C where the leak rates dropped to 0.30 and 7.50 cm^3/min, respectively. A 120-minute air purge was performed on each membrane the morning after the furnace reached temperature. After the air purge, the leak rates were 1.55 and 6.10 cm^3/min. These leak rates are accounted for in calculating the fluxes. At 400°C and 20 psid, the fluxes were 14.5 and 17.3 $cm^3/cm^2 \cdot$min before an air purge and 20 and 21 $cm^3/cm^2 \cdot$min after a 120-minute air purge.

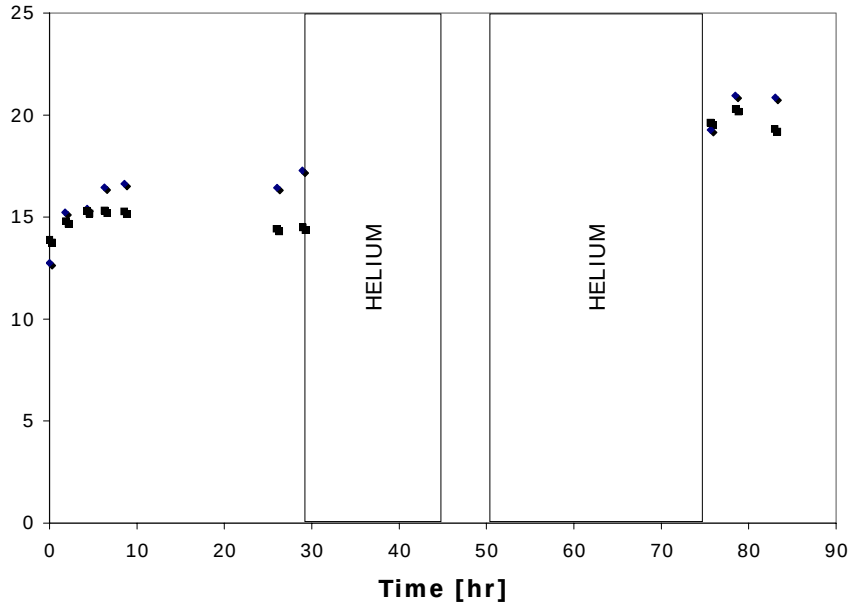

Figure 54. Pure hydrogen flux versus time for batch 032406#1

The effects of performing an air purge once the membrane reaches temperature can be seen by comparing Figure 53 and Figure 54. The samples from batch 051206#1 took about 80 hours to reach steady state (Figure 52) while batch 032406#1 took about 28 hours (Figure 53).

Four samples with an estimated composition of 62% palladium (batches 072806#1 and 073106#1) tore during preparation for testing. Two of the samples tore while being cut and the other two tore when pressure was applied during sealing. Two more samples, 072806#1 and 073106#1, were annealed in forming gas at 400°C for 24 hours.

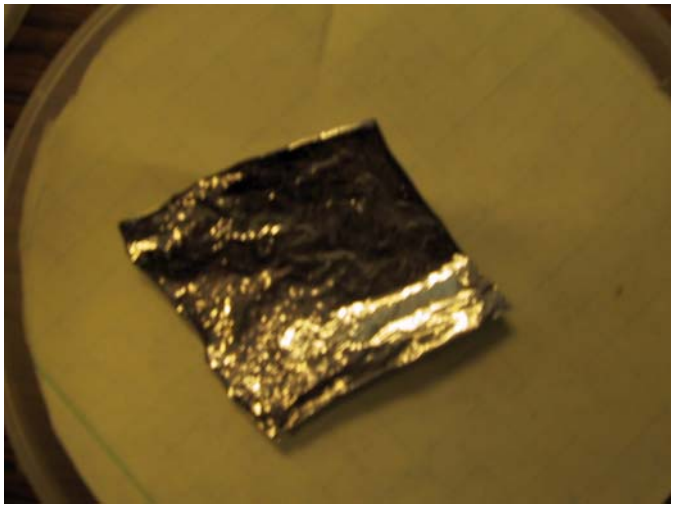

Figure 55. Sample 073106#1 after 24 hours at 400°C in forming gas

As can be seen in Figure 55, a significant amount of wrinkling occurred during annealing. Although it can not be seen in Figure 55 there was also portions of the membrane that were copper colored. These sections were found in the more wrinkled part of the membrane (left side of membrane in Figure 55).

A ternary membrane (PdCuTa) was tested for 5 days at 400°C. The sample was heated to 400°C in helium where a one hour 30 minute air purge was performed. The sample had a helium leak and the H_2/He selectivity was about 17. The permeability, corrected for the helium leak using Knudsen diffusion, reached a maximum value of 9.85×10^{-6} $cm^3(STP) \cdot cm/cm^2 \cdot s \cdot cmHg^{0.5}$ at 400°C and 20 psid but was decreasing as the test continued. After approximately 5 days the feed was switched to helium so an air purge could be performed. The membrane tore when the feed was switched to helium so the air purge was never completed. The final value of the permeability was 4.95×10^{-6} $cm^3(STP)cm/cm^2 \cdot s \cdot cmHg^{0.5}$. This value is much closer to the values obtained for the other ternary alloys, PdCuRh (2.46×10^{-6}) and PdCuRu (3.52×10^{-6}). Figure 556 shows the pure hydrogen flux versus time for sample 032006#1.

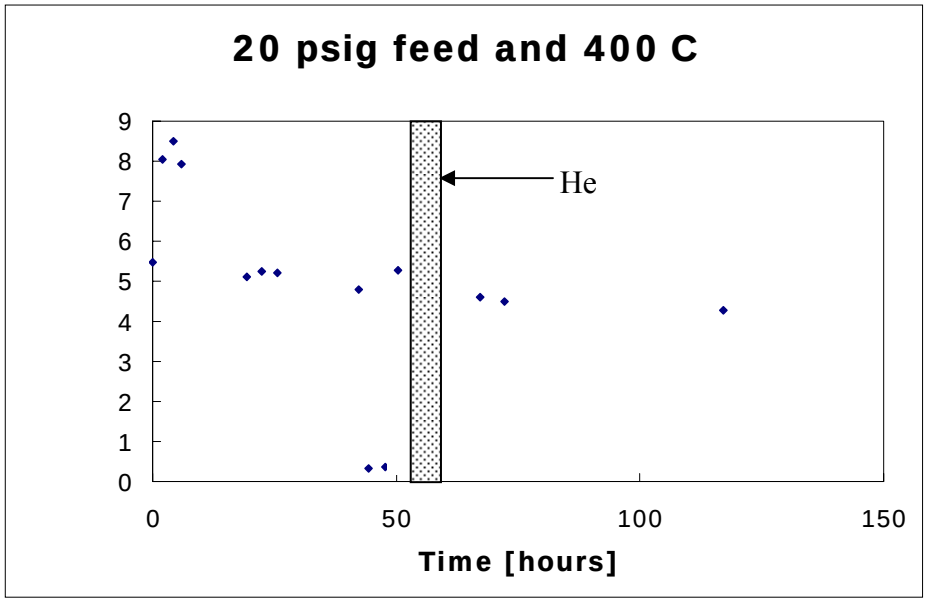

Figure 56. Pure hydrogen flux versus time for ternary sample 032006#1

Membrane 072806#1 was tested for 5 days. The H_2/He selectivity of the membrane was poor, 4.3, since the membrane had a few pinholes. More importantly was the test of the new diffusion barrier. A 50 nm coat of tantalum oxide was deposited onto the surface of the porous stainless steel support disc. The layer did not hinder the flow through the disc so sample 072806#1 was placed in the test fixture on the coated support. After 5 days the test was stopped and the sample removed. The membrane came off the stainless disc without any force. The membrane not sticking to the disc shows that the tantalum oxide layer provided resistance against diffusion bonding. Another significant result was the lack of tearing in the sample.

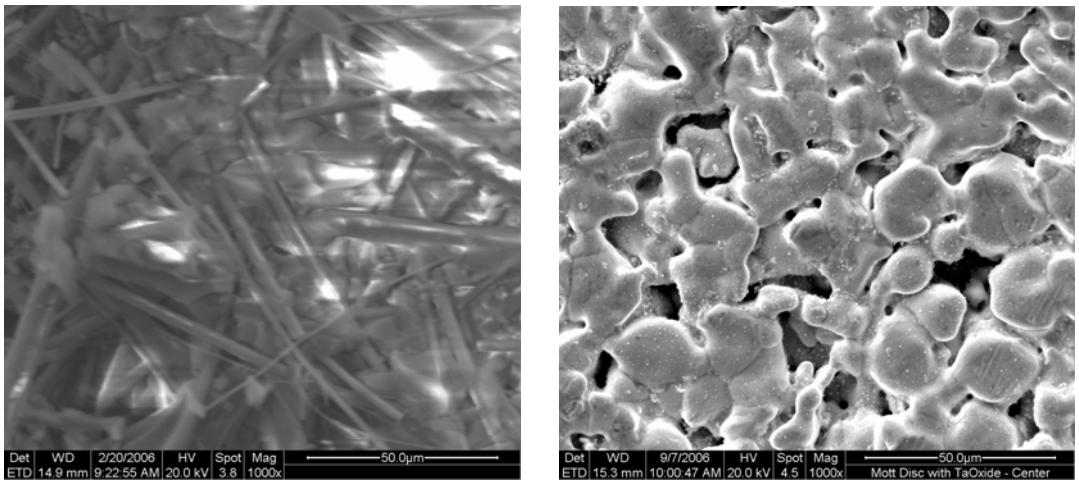

a) b)

Figure 57. a, b – SEM images of ceramic paper and tantalum oxide coated stainless steel

As can be seen in Figure 57a and 57b, the surface of the tantalum oxide does not have any sharp points. The thinner membranes, this batch especially, tore when sealed into the test apparatus. The tear was around the outside where the fixture applied a pressure to the graphite seal. The ceramic paper poked through the membrane causing a defect. When the membrane was introduced to gas at any pressure, the defect from sealing opened and ruined the membrane. Batch 072806#1 tore in this manner before, but when used with the tantalum oxide coated disc the membrane sealed and no tears were present after testing. The tantalum oxide layer shows promise as a diffusion barrier in that EDAX measurements on the surface of the stainless steel disc showed no palladium or copper. Also, the surface of the oxide layer was more spherical which gives more area for contact between the layer and the membrane. This reduced the amount of tearing in the membrane and allowed for testing of thin (<5 μm) membranes.

Membrane 073106#1 was tested for 6 days. The membrane had a slight helium leak, 0.80 cm^3/min, but the Knudsen corrected hydrogen flux was about 19 cm^3/min. The membrane was heated to 400°C in helium and then air purged once at temperature.

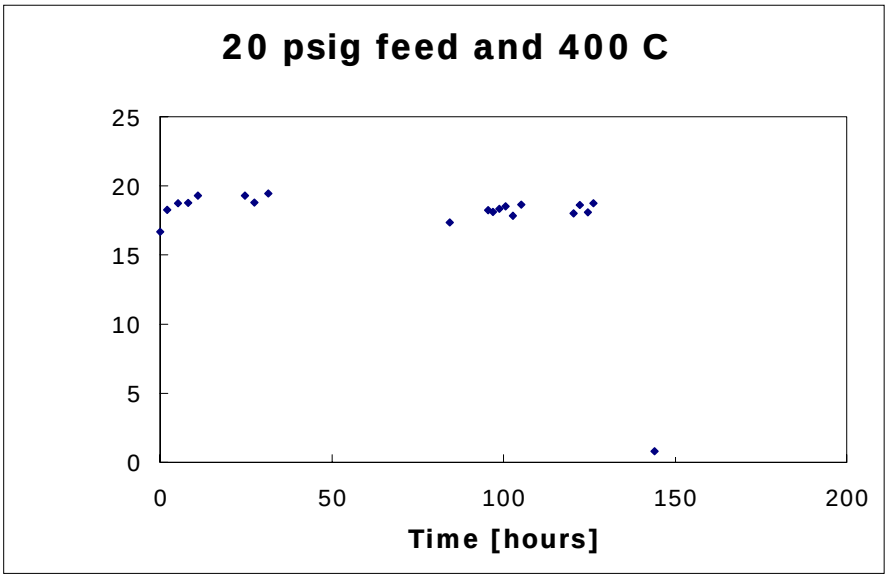

Figure 58. Hydrogen flux versus time for membrane 073106#1

As can be seen in Figure 58, once the membrane was exposed to hydrogen after the air purge it reached a steady value within a day. This membrane had a Knudsen corrected permeability of 2.84×10^{-5} cm^3(STP)cm/cm^2·s·$cmHg^{0.5}$ at 400°C and 20 psid. This value is low and probably due to the composition. This was the 62%Pd sample and the membrane was high in palladium putting it on the opposite side of the peak in permeability versus alloy composition as the previous samples.

Module Construction and Testing

IdaTech inspected several experimental membranes and in some instances discovered pinholes that were not revealed in light box tests at SwRI. While it is possible that pinholes developed during cutting of the membranes to size or during shipment, IdaTech returned selected samples for SwRI

to re-inspect. Small 1-inch diameter active area foils from a 5 μm thick sample were provided by SwRI for initial pressure testing. The apparatus used was a permeation cell (Figure 59) heated in a furnace. The sample was pressurized to 1000 psig and operated without failure for several hours. The hydrogen flux was measured while at 400°C and under 100 psig H_2. Hydrogen flux was 421 SCFH/ft^2, which is consistent with estimated values based on the thickness.

Figure 59. IdaTech permeation cell used in initial pressure testing of thin membranes

Figure 60 is a photograph picture of the full-scale prototype purifier designed to deliver 5 L/min of hydrogen. The first attempt to build up a reformer/membrane module using this hardware with a 6 μm SwRI membrane failed during the gasket compression step of assembly. Figure 61 shows a photograph of the failed membrane. Inspection of the membrane outer edges (sealing region) shows many small tears, one of which extends into the active region of the membrane. This membrane was not annealed prior to assembly. No difficulties were encountered in assembling a reformer/membrane module a 5 μm rolled foil which was leak tested without failure. In order to get a leak tight assembly, very high gasket loadings are required which in combination with a support material that is not flat can result in failure of an insufficiently flexible membrane.

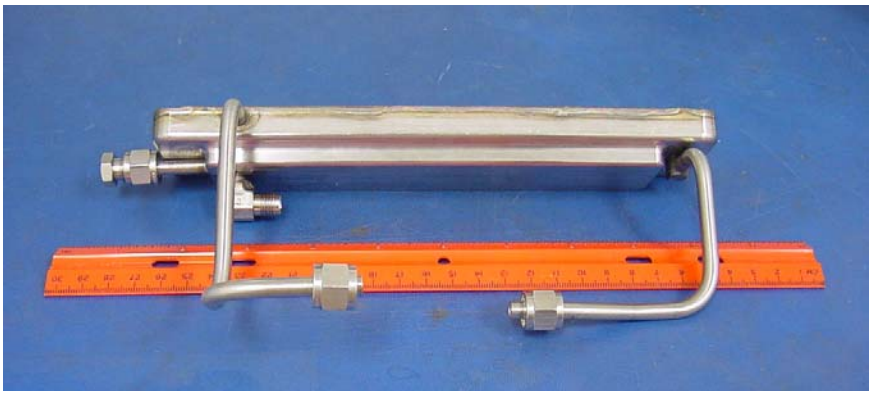

Figure 60. IdaTech's prototype membrane module

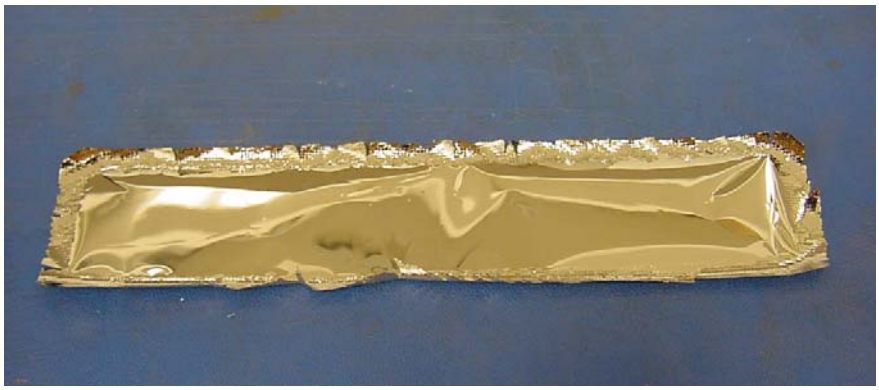

Figure 61. Photograph of compress membrane that developed a tear upon compression

Figure 62 shows full-size membranes before and after annealing. Invariably, some degree of wrinkling was observed in the foil after annealing, although the foils tended to lay flatter suggesting that the heat treatment had relieved much if not all of the residual stress present in the as-deposited membrane. Several of the annealed membranes were inspected for the presence of pinholes with passing samples supplied to IdaTech.

Figure 62. Full-size membranes before (foreground) and after (background) annealing in argon for 12 hours at 450°C.

IdaTech's focus on commercial product development has centered around cost reduction and reliability improvement. With respect to the 250W iGen™ fuel cell system, the work has been focused on redesign of the fuel processor (reformer and hydrogen purification), long term testing of the new designs and certification of the final product.

At a meeting in September 2007 between IdaTech and SwRI, the issues of pinholes, flatness and brittleness of the SwRI supplied foil were discussed and the following action items were generated:

1) SwRI to try to re-anneal membrane samples that had previously been sent to IdaTech.
2) SwRI to try to coat Pd40Cu directly on the IdaTech support material.

3) IdaTech to try to assemble membrane module with previously annealed foil from SwRI to see if previous annealing method relieved stresses in the membrane enough to prevent shattering during cutting and gasket compression.
4) If IdaTech unsuccessful with previously annealed membrane, try again with re-annealed material from action item 1.
5) If IdaTech successful with assembly of a membrane module, then generate hydrogen from methanol and water.

SwRI re-annealed membrane samples and sent them to IdaTech for testing. The results were mixed and suggest that the annealing step had promise, but needed to be optimized. General observations of the annealed material:

- The annealing process appeared to create pinholes in the membrane. Membranes that had been returned to SwRI for annealing that had few or no pinholes had an increase in the number of pinholes after the annealing step.
- The annealed membranes were stress-relieved enough to prevent shattering of the membrane during trimming steps, but still failed during the gasket compression step. The required gasket compression required for sealing the membrane can be revisited, but it is based on extensive testing by IdaTech. Lower gasket loading could be used, but the result will be membrane modules with higher leak rates.
- IdaTech was not able to successfully assemble a module that would meet IdaTech's allowable leak rate requirements and did not pursue assembly of a fuel processor with the SwRI membrane.

The principle criteria that IdaTech used to determine suitability of the foil for use in a membrane module (assuming that the material had met the alloy composition specifications) are:

- Foil must be flat – ripples in the membrane lead to formation of wrinkles that will ultimately result in mechanical fatigue failures.
- Foil must be defect free – no pinholes.

Four membrane samples were returned to SwRI for additional annealing. The foils were all light-boxed to check for pinholes prior to being sent to SwRI. The table below gives before and after light box results:

Table 9. Foil Inspection Before and After Annealing

Sample I.D.	Pinholes Before	Pinholes After	Comment
5/18/06 #1	11	15	Went from flat to highly stressed
5/19/06	3	4	Ripples in the foil before and after
5/11/06 #1	1	2	Ripples in the foil before and after
5/12/06 #1	0	3	Foil flat

An example of foil that was not flat is shown in the figure below. In this case the foil was not flat before or after annealing. The current annealing process did not remove the wrinkles.

Figure 63. Sample 5/11/06 #1 Showing Ripples (Non-flatness)

Figure 63 shows sample 5/18/06 #1 that went from flat prior to the annealing step to highly stressed after the annealing step. The membrane rolled up on itself and did not lay flat which made it very difficult to handle and put into a membrane module.

Figure 64. Sample 5/18/06 #1 Showing High Stress

Figure 65 through 68 show a sampling of various defects observed on Sample 5/12/06 #1. It was suspected that the surface defects or structure defects while not initially detected under a light box open up during the annealing step. It would not be practical to inspect every foil sample under a microscope looking for defects prior to assembling a membrane module. The source of the defects must be identified and appropriate corrective action taken to prevent the formation of these defects.

Figure 65. Pinhole Example

Figure 66. Example of a Large Pit

Figure 67. Examples of Spongy Areas

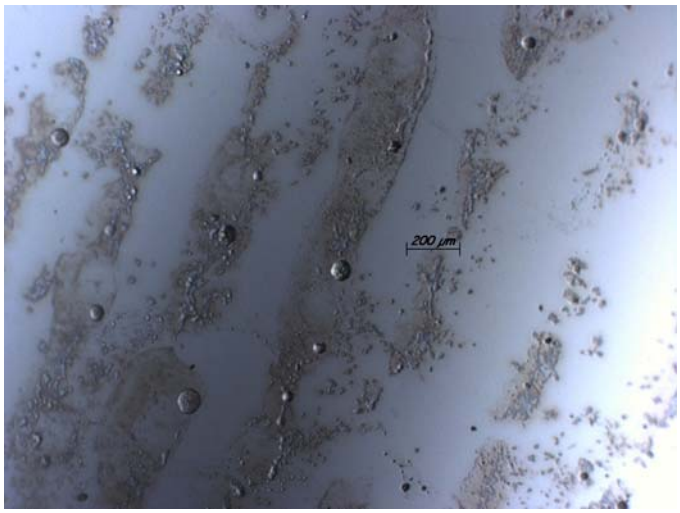

Figure 68. Example of Surface Defects

A decision was made to build up a membrane module with the best of the foils and see if the annealed foil was sufficiently annealed to prevent damage during the gasket compression step. Sample 5/23/06 #1 was put into a membrane housing and then compressed to form a gasket seal. The leak rate of the compressed assembly could not be measured, so the membrane was removed and examined on the light box. Prior to the gasket compression step, the membrane had 3 pinholes. After the gasket compression step, 17 pinholes were identified. The majority of the pinholes are located around the periphery of the membrane where the gasket seal is made. A pinhole in the gasket area is not necessarily bad, unless it is too close to the active membrane area. Looking at Figure 69, the dimpled area around the periphery of the membrane shows the gasket location. The circles show locations of pinholes.

Figure 69. Sample 5/23/06 #1 After Gasket Compression (Circles on membrane show location of pinholes)

The present IdaTech module manufacturing process is not capable of utilizing the SwRI thin film membranes to fabricate a prototype hydrogen purification system. The following areas for foil development have been identified.

- The annealing step shows promise in reducing membrane stresses, but needs to be further optimized.
- There are still issues with pinholes that need to be addressed. Source of the defects need to be identified and corrected.
- There also needs to be some process optimization to form flat membranes.

For module development, the following areas for future development have been identified.

- Alternative gasket compression methods.
- Identification and remediation steps for pinhole formation at gasket/membrane interface.
- Review and modification of the module design to accommodate thin membranes.

These areas for development will not be completed in the present program and will require future investment to be investigated.

The annealed membranes were stress-relieved enough to prevent shattering of the membrane during trimming, but failed during the gasket compression step. The required gasket compression for sealing the membrane is based on extensive testing by IdaTech and lower gasket loading could be used, since the resulting membrane modules exhibit higher leak rates. IdaTech was not able to successfully assemble a module that would meet IdaTech's allowable leak rate requirements and did not pursue assembly of a fuel processor with the SwRI membrane. Fabrication of a module utilizing the SwRI foils will require significant development of a new gasket compression process or alternative module design.

Process Cost Analysis

Of the elements that comprise a hydrogen purification module, the membrane is presumed to be by far the most significant cost contributor. Analogous to a computer's central microprocessor, the membrane lies at the heart of the purification system and is the key element defining system performance. The DOE has set aggressive performance and cost targets for several membrane properties in 2005 and 2010 including flux, cost per square foot, hydrogen purity, and differential pressure.

Vacuum deposition methods for rolled products, commonly referred to as "web coating," have been applied for more than 20 years. Metal films, typically only a few hundred Angstroms thick, can be deposited onto film up to several meters wide with a uniformity of better than 10%. Typical costs for manufacture of metallized plastic (e.g., aluminum on PET) can be less than a penny per square meter of material while production volumes for a single production web coater can exceed 100 million square meters a year. The fixed cost invested for this technology, however can be considerable, with production machines costing several millions of dollars to design and construct. Figure 70 shows the relative cost contribution of several key factors to the operating cost for a typical aluminum metallizer as estimated by Broomfield [6].

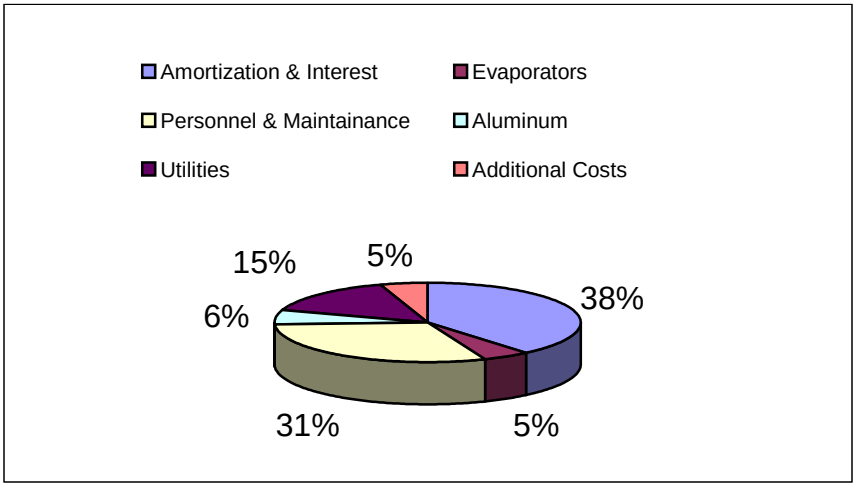

Figure 70. Relative cost contributions to operation of a conventional web coating system.

For Pd alloy membrane fabrication the materials cost is expected to be higher relative to other fixed costs. Another key element impacting the cost is material throughput. If a greater square footage of material the can be produced over a given time, the labor and capital equipment costs can be substantially reduced. This has been verified for vacuum-based sputter deposition processes used in the semiconductor industry [7]. It is likely a semiconductor process tool can be adapted to produce full-size Pd alloy membranes up to 12 inches in diameter. The membrane throughput for such a system can be estimated to first order using the following empirical equation.

$$\#\ ft^2/min = 0.785\ \ N\ D\ /\ d$$

Where N is the number of process stations, D is the deposition rate (nm/min) and d is the target membrane thickness in nm. A typical system can allow up to 5 12-inch wafers to be processed simultaneously and deposition rates of 600nm/min are possible. So for a membrane thickness of 4 microns (4000nm), 0.59 sq. ft. of membrane per minute can be produced. Obviously, this estimate neglects the contributions of cycle time and downtime due to maintenance although these may be included by altering the above equation in the following manner.

$$\#\ ft^2/min,\ P = 0.785\ \ N\ D\ U\ (1\text{-}C)\ /\ d$$

Where U is the average uptime percentage and C is the percentage of time in each cycle where material is not being deposited. Assuming 75% uptime and 25% coating cycle idle time, then 0.33 sq ft/min of membrane will be produced on average.

The next issue to consider is raw materials cost. The cost of palladium greatly exceeds that of copper so we can reasonably omit the later from consideration. Sputter deposition processes are highly efficient with more than 95% of sputtered material typically deposited on the support material in a production system. The balance of the material can be recovered as scrap and

recycled. The other cost consideration if fabrication of the Pd-Cu alloy target. This is usually done by taking powders of each material in appropriate quantity to make the desired alloy composition then hot pressing the power in vacuum or inert atmosphere to make a plate, typically 0.5 inches thick. For this calculation an additional 25% is added to the cost of palladium for target manufacturing and material recovery. Based on this as well as the composition, density, and thickness of the membrane and market price of Pd, the membrane raw materials cost per square foot can be calculated using the following empirical equation

$$\text{Raw materials cost/ft}^2,\ R = 1.2 \times 10^{-2}\ P\ W\ (W+3)\ T$$

Where P is the market price ($/oz), W is the weight percentage, and T is the membrane thickness in microns. Hence a 4 micron thick, 60 wt. % Pd alloy membrane with a market price of $330/oz, will have approximately $35/ft^2 of Pd in it. Combine this information with the projected material throughput and a total cost for manufacturing based is constructed based on the following factors.

$$\text{Total Cost/ft}^2 = (F + L + E) / (P*S*1.75 \times 10^5) + R$$

Where F is the annual equipment depreciation, L is the fully burdened annual labor costs, E is the annual cost of utilities and maintenance, P is the throughput per minute, and S is the number of 8 hour shifts per day. If a $1.5M piece of equipment with level amortization over 3 years, 4 full time personnel (3 technicians and 1 engineer) working a total of 2 shifts at $0.50M/yr, and $0.20M/yr in utilities and maintenance are assumed including the above estimates for productivity and raw materials, a total cost of $45.40 per square foot is calculated. Even if the throughput, equipment, or labor costs have been significantly underestimated, this cost estimate is more than an order of magnitude lower than the DOE 2010 target, which indicates that the process will be cost effective.

CONCLUSION

Self-supporting Pd-Cu alloy membranes have been produced with thicknesses down to 3 μm. Hydrogen permeability rates in excess of the 2010 DOE Targets have been measured and self-supporting membranes that exhibit long life at temperatures above 300°C were produced. It has been shown to be feasible to produce membranes below 5 μm in thickness that are cost competitive with other methods for hydrogen separation in energy applications. The program is well positioned for pilot scaling and membrane incorporation in commercial separation units.

REFERENCES

1. Gryaznov, V.M. Catalysis on permselective membranes. Doklady Akademii Nauk SSSR **1969**, *189(4),* 755.
2. Mohan, K; Govind, R. Analysis of Equilibrium Shift in Isothermal Reactors with a Permselective Wall. AIChE J. **1988**, *34(9),* 1493.
3. Tylkina, M.A.;Tsyganova, I.A. Properties of Pd-Rh alloys. Russ J. Inor. Chem**. 1963***, 8(10),* 1229.

4. Saubestre, E.B. Electroless Plating Today. Metal Fin**. 1962**, *60(9),* 59.
5. Andrew, P.L.; Haasz, A.A. Effect of thin copper and palladium films on hydrogen permeation through iron. J. Less-Common Met. **1991**, *172-174*, 732.
6. A. A. Broomfield, Society of Vacuum Coaters, Annual Technical Conference Proceedings **1992**, 21.
7. S. Edelstein, R. Davenport, and J. Nulman, Proc. SPIE Vol. 2336, p. 162-168, Manufacturing Process Control for Microelectronic Devices and Circuits, Anant G. Sabnis; Ed, 1994.